



HAL
open science

Arctic and Antarctic Sea Ice Thickness and Volume Changes From Observations Between 1994 and 2023

Marion Bocquet, Sara Fleury, Frédérique Rémy, Fanny Piras

► **To cite this version:**

Marion Bocquet, Sara Fleury, Frédérique Rémy, Fanny Piras. Arctic and Antarctic Sea Ice Thickness and Volume Changes From Observations Between 1994 and 2023. *Journal of Geophysical Research: Oceans*, 2024, 129, pp.2023JC020848. 10.1029/2023JC020848 . insu-04835175

HAL Id: insu-04835175

<https://insu.hal.science/insu-04835175v1>

Submitted on 13 Dec 2024

HAL is a multi-disciplinary open access archive for the deposit and dissemination of scientific research documents, whether they are published or not. The documents may come from teaching and research institutions in France or abroad, or from public or private research centers.

L'archive ouverte pluridisciplinaire **HAL**, est destinée au dépôt et à la diffusion de documents scientifiques de niveau recherche, publiés ou non, émanant des établissements d'enseignement et de recherche français ou étrangers, des laboratoires publics ou privés.



Distributed under a Creative Commons Attribution 4.0 International License

Arctic and Antarctic Sea Ice Thickness and Volume Changes From Observations Between 1994 and 2023

Marion Bocquet^{1,2} , Sara Fleury¹, Frédérique Rémy¹, and Fanny Piras² 

¹Université de Toulouse, LEGOS (CNES/CNRS/IRD/UT3), Toulouse, France, ²Collecte Localisation Satellites (CLS), Toulouse, France

Key Points:

- A 30-year data set from four satellite radar altimeters provides the longest sea ice thickness record for both polar regions
- Arctic sea ice is significantly thinning for each month of the year, whereas Antarctic undergoes complex regional thickness changes
- Sea ice volume variability can be explained by sea ice thickness variability in both polar hemispheres

Supporting Information:

Supporting Information may be found in the online version of this article.

Correspondence to:

M. Bocquet,
marion.bocquet.legos@gmail.com

Citation:

Bocquet, M., Fleury, S., Rémy, F., & Piras, F. (2024). Arctic and Antarctic sea ice thickness and volume changes from observations between 1994 and 2023. *Journal of Geophysical Research: Oceans*, 129, e2023JC020848. <https://doi.org/10.1029/2023JC020848>

Received 20 DEC 2023

Accepted 23 SEP 2024

Author Contributions:

Conceptualization: Marion Bocquet

Funding acquisition: Fanny Piras

Methodology: Marion Bocquet

Software: Marion Bocquet

Supervision: Sara Fleury, Frédérique Rémy, Fanny Piras

Validation: Marion Bocquet

Visualization: Marion Bocquet

Writing – original draft: Marion Bocquet

Writing – review & editing: Sara Fleury, Frédérique Rémy, Fanny Piras

© 2024. The Author(s).

This is an open access article under the terms of the [Creative Commons Attribution License](https://creativecommons.org/licenses/by/4.0/), which permits use, distribution and reproduction in any medium, provided the original work is properly cited.

Abstract Both Arctic and Antarctic sea ice are affected by climate change. While Arctic sea ice has been declining for several decades, Antarctic sea ice extent slowly increased until 2015, followed by a sharp drop in 2016. Quantifying sea ice changes is essential to assess their impacts on the ocean, atmosphere, ecosystems and Arctic communities. In this study, we combine sea ice thickness estimates from four satellite radar altimeters to derive the longest time series of homogeneous sea ice thickness for both hemispheres over 30 years (1994–2023). The record supports the rapid loss of sea ice in the Arctic for each month of the year and the heterogeneous changes in sea ice thickness in the Antarctic. The study confirms that most of the volume variability is due to the thickness variability, which holds true for both hemispheres. The sea ice thickness time series presented here offer new insights for models, in particular the possibility to evaluate sea ice reanalyses and to initialize forecasts, especially in the Antarctic, where the data set presented here has no equivalent in terms of spatial and temporal coverage.

Plain Language Summary Arctic and Antarctic sea ice respond significantly to climate change, as documented by decades of satellite records of sea ice coverage. Arctic sea ice coverage has declined steadily over the past 40 years, while Antarctic sea ice coverage increased until 2016, followed by a rapid decline. In contrast, changes in sea ice thickness, which contribute to changes in sea ice volume, are much less well documented due to the lack of long-term observations. In this study, we address this gap by producing a 30-year time series of sea ice thickness (1994–2023) using data from four satellite radar altimeters, representing the longest consistent data set for both polar regions. This was made possible by using machine learning to align the different satellite missions and incorporating an ensemble of snow depth products to cover the entire period. The resulting time series shows a rapid decrease in Arctic sea ice thickness over the study period. In contrast, Antarctic sea ice shows thickness changes with significant spatial variability. This new data set provides critical insights into sea ice dynamics, their causes, and their impacts on climate, ecosystems, and Arctic communities.

1. Introduction

Ice in its various forms is often used as an indicator of the effects of climate change. Sea ice is currently undergoing perhaps the most dramatic and profound changes. The history of Arctic sea ice is well documented; its extent has been declining for the past four decades (J. C. Comiso et al., 2017; W. N. Meier et al., 2014; Stroeve & Notz, 2018). The IPCC (Intergovernmental Panel on Climate Change) 6th report predicted an ice-free Arctic Ocean in the 2050s (Notz & SIMIP Community, 2020), which has been recently revised to the 2030s–2050s (Kim et al., 2023). The Antarctic, considered a polar opposite (Maksym et al., 2012), reflects more complex and contrasting changes, with an increase in ice extent observed until 2016, followed by an abrupt decline, bringing the ice to a new state with a series of record lows. The drivers of these recent changes are not well understood (Eayrs et al., 2021), but recent warming of ocean temperatures is considered a contributing factor (Purich & Doddridge, 2023). Sea ice thickness plays a key role in the evolution of sea ice, but this key climate variable remains poorly observed in long-term records. Satellite altimeter observations provide extensive spatial coverage, particularly in the Southern Ocean where sea ice is outside the polar gap due to satellite orbit limitations. However, robust quantification of monthly sea ice thickness changes has only been possible since the launch of the CryoSat-2 mission in 2010, a capability that has been further enhanced by the ICESat-2 (Ice, Cloud, and land Elevation Satellite) mission (Fons et al., 2023; Kacimi & Kwok, 2020; Kwok et al., 2020; Landy et al., 2019, 2022; S. W. Laxon et al., 2013; Ricker et al., 2018; R. L. Tilling et al., 2018). This includes analysis of data from legacy missions such as European Remote Sensing (ERS) and Envisat. While sea ice thinning in the central Arctic has been well established for over 40 years using submarine data (Kwok, 2018; Kwok et al., 2009), monthly

Arctic and Antarctic-wide estimates are only available for a short period (2002–2017) by combining the Envisat and CryoSat-2 missions (Guerreiro et al., 2017; Paul et al., 2018; Schwegmann et al., 2016). An attempt was made to estimate the thickness was made with the ERS missions (S. Laxon, 1994; S. Laxon et al., 2003; Giles et al., 2008), but no further studies have been carried out since then. Past missions, ERS-1, ERS-2 and Envisat, carried conventional pulse-limited radar altimeters (RA and RA-2), whose measurements are more affected by surface roughness than delay-doppler or synthetic aperture radar (SAR) altimeters, such as the SAR Interferometric Radar Altimeter (SIRAL) on board CryoSat-2 (Chelton et al., 1989; Raney, 1998). Conventional altimeters use a single pulse for each measurement, resulting in a larger footprint. In contrast, SAR altimetry transmits bursts of pulses at a high rate and uses the Doppler effect to achieve a much narrower footprint along the satellite's track. To date, the use of these missions has required homogenization of the radar freeboard with CryoSat-2 data, but the methods (Guerreiro et al., 2017; Paul et al., 2018; R. Tilling et al., 2019) have only focused on Envisat retrievals. Recently, we have been able to retrieve the monthly sea ice thickness for the Arctic from the European Space Agency's (ESA) legacy mission ERS-2 (Bocquet et al., 2023), providing the opportunity to recover 30 years of near-basin-wide estimates. A preliminary study (Garnier et al., 2022) demonstrated the ability of the method to be applied to the Antarctic for Envisat.

This study aims to use the four ESA missions ERS-1, ERS-2, Envisat and CryoSat-2 (CS-2) to present 30 years of consistent and homogeneous monthly sea ice thickness and volume variations over the Arctic and Southern Oceans. A detailed uncertainty quantification using an ensemble approach supports the retrieval of monthly sea ice thickness. The resulting time series are used to estimate regional trends in thickness as well as global and regional volumes. The role of thickness variability in volume changes is also assessed, followed by an overview of changes in the contribution of ice thickness to volume changes.

2. Data and Methods

2.1. From Radar Freeboard to Sea Ice Thickness Estimation

We use the ERS-1, ERS-2, Envisat, and CryoSat-2 L1B waveforms up to 81.5°N/S (due to orbit limitations) with a sampling rate of 300 m along the ground track of the satellites to retrieve radar freeboard. Radar freeboard is defined as the difference between the elevation of sea ice floes above the local sea surface measured in the leads. Each waveform is classified as corresponding to either a lead or a sea ice floe using Pulse Peakiness (PP) (Bocquet et al., 2023; S. Laxon et al., 2003; Peacock & Laxon, 2004), defined as:

$$PP = \frac{\max(WF)}{\sum_{i=0}^{Nb_{WF_{bins}}} \cdot WF_i}$$

Pulse peakiness thresholds are taken from Bocquet et al. (2023), with ERS-1 and ERS-2 sharing the same thresholds. The CryoSat-2 data set is processed from L1b Ice products, while for the Envisat and ERS missions, we use the RA-2 Sensor and Geophysical Data Record (SGDR) and the RA REAPER Sensor and Geophysical Data Record data sets, both accessible from the ESA data portal. Our analysis focuses on data collected during the winter months (October–April) for the Arctic and year-round for the Antarctic. The measurements are gridded for each calendar month at a resolution of 12.5 km. For each grid cell, estimates are selected within a smoothing radius of 25 km during the desired month. Uncertainties are used as weights in the weighted mean calculation to produce monthly radar freeboard maps (Bocquet et al., 2023). Sea ice thickness (SIT) is derived from altimetry-based Ku-band radar freeboard, following the methodology of (S. Laxon et al., 2003). Sea ice thickness is calculated from the ice freeboard (“emerged part of the ice,” FB_i), the snow depth (h_s) and the densities of sea ice (ρ_i), sea water (ρ_w) and snow on sea ice (ρ_s), assuming that the sea ice is in hydrostatic equilibrium (see Equation 1).

$$SIT = \frac{\rho_w}{\rho_w - \rho_i} \cdot FB_i + \frac{\rho_s}{\rho_w - \rho_i} \cdot h_s \quad (1)$$

Several biases contribute to the estimation of sea ice freeboard, including surface roughness, misidentification of the first maximum, effectiveness of sea ice waveform classification in mixed conditions, and uncertainty in actual snow conditions for range corrections. We believe that the cumulative effect of all biases with this approach should provide an approximation of mean sea ice freeboard.

Radar altimetry is also affected by the snow layer, which slows down the speed of the signal. The radar freeboard (FB_r) must be corrected for this effect to determine the sea ice freeboard (Equation 2) (Mallett et al., 2020), with $c/c_s = (1 + 0.00051 \cdot \rho_s)^{1.5}$ (Ulaby et al., 1986).

$$FB_i = FB_r + h_s \cdot (c/c_s - 1) \quad (2)$$

2.1.1. Radar Freeboard (FBr)

The CryoSat-2 radar freeboard is estimated following the method presented in S. W. Laxon et al. (2013), using a Threshold First-Maximum Retracker Algorithm (TFMRA) retracker (Helm et al., 2014) with a fixed threshold set at 50% for both the lead and the floe to ensure consistency with the legacy missions of ERS-1, ERS-2, and Envisat. The three former missions operate in Low Resolution Mode (LRM). Unfortunately, this mode is poorly understood over sea ice, resulting in more challenging and potentially biased measurements. LRM measurements have a larger footprint than SAR mode and depend on surface roughness. The rougher the sea ice surface, the larger the footprint (Chelton et al., 1989), resulting in higher sensitivity to surface heterogeneity, especially with residual mixed surface types (causing snagging) and volume backscattering (Guerreiro et al., 2017). This issue is addressed by calibrating legacy missions over CryoSat-2, taking advantage of the mission overlap periods. In this study, the calibration is performed using a neural network (Bocquet et al., 2023) based on sea ice surface state and properties. This ensures the continuity of the radar freeboard between all missions. For the Antarctic, the same methodology has been applied without the information on sea ice type, as introduced by Garnier et al. (2022).

Radar freeboard and thickness estimates are removed when the sea ice concentration is less than 50%. Estimates in the Marginal Ice Zone (MIZ) are excluded to avoid the effects of swell. All statistics in this study follow this restriction for both hemispheres, which affects the calculation of the sea ice volume. It is important to note that the sea ice area with concentrations below 50% represents less than 3% of the total sea ice area for the Arctic and less than 7% for the Antarctic during winter. As this sea ice is more likely to be thinner, global or regional statistics (including MIZ) may be overestimated. To maintain consistency throughout the study, this restriction is applied to all additional data sets and comparisons that involve volume.

2.1.2. Densities

The density of seawater is chosen to be $\rho_w = 1024 \text{ kg} \cdot \text{m}^{-3}$, with the corresponding uncertainty $u_{\rho_w} = 0.5 \text{ kg} \cdot \text{m}^{-3}$ (Alexandrov et al., 2010).

For the Arctic: ρ_i , the sea ice density is estimated from the sea ice freeboard according to the parameterization of Jutilla et al. (2022). While proper uncertainties for the sea ice density are not published with this parameterization, uncertainties for the regression coefficients are available and are used to generate an ensemble of sea ice densities (see Section 2.3). The snow density ρ_s is chosen to be $\rho_s = 300 \text{ kg} \cdot \text{m}^{-3} \pm 50 \text{ kg} \cdot \text{m}^{-3}$ if snow depth observations are used, otherwise the snow density from the snow model is used.

Note that the parameterization of Jutilla et al. (2022) leads to a higher estimate of sea ice thickness compared to previous studies (Guerreiro et al., 2017; Landy et al., 2022; Paul et al., 2018; Ricker et al., 2018) due to a higher sea ice density on multi-year ice than the commonly used but underestimated sea ice density of Alexandrov et al. (2010) and Jutilla et al. (2022) (see Figure A5 to note the effect of snow density parameterization on sea ice volume).

For the Antarctic: Sea ice density is used depending on the season according to N. T. Kurtz and Markus (2012) based on Maksym and Markus (2008). $\rho_i = 920 \text{ kg} \cdot \text{m}^{-3}$ for winter, $900 \text{ kg} \cdot \text{m}^{-3}$ for autumn and spring, and $875 \text{ kg} \cdot \text{m}^{-3}$ with the corresponding uncertainty of $20 \text{ kg} \cdot \text{m}^{-3}$. Snow density is also seasonally variable, $330 \text{ kg} \cdot \text{m}^{-3}$ for winter, $340 \text{ kg} \cdot \text{m}^{-3}$ for autumn, $320 \text{ kg} \cdot \text{m}^{-3}$ for spring and $350 \text{ kg} \cdot \text{m}^{-3}$ (N. T. Kurtz & Markus, 2012) during summer with the corresponding uncertainty of $70 \text{ kg} \cdot \text{m}^{-3}$ (Kacimi & Kwok, 2020).

2.1.3. Snow Cover—An Ensemble Approach for Estimating Sea Ice Thickness

There is no long-term continuous record of snow depth available at the basin scale for either hemisphere covering the last 30 years (1994–2023). Snow cover is therefore a major challenge in estimating sea ice thickness for our study. However, a variety of snow depth and density data sets are available, including those from models and

observations collected with different sensors and processing methods. Although this diversity reveals significant discrepancies between sea ice thickness (SIT) and volume estimates, it also provides an opportunity to reduce uncertainty by using multiple sources. This study addresses this challenge by using an ensemble of snow depth products to compute a corresponding ensemble of SITs. The number of members in the ensemble varies depending on the time period and availability of the data sets.

To combine these estimates, we use a weighted mean SIT (SIT_{wm}), which is calculated as the weighted average of the individual SIT estimates (SIT_k) (see Equation 3)

$$SIT_{em} = \sum_{k=1}^N w_k \cdot SIT_k \quad (3)$$

The weight w_k is equal to the inverse uncertainty on SIT_k induced by the snow depth and density $w_k^{-2} = \frac{\partial SIT_k^2}{\partial \rho_s^2} \cdot u_{\rho_s}^2 + \frac{\partial SIT_k^2}{\partial h_s^2} \cdot u_{h_s}^2$. Note that u_{ρ_s} and u_{h_s} represent the uncertainties in snow density and snow depth, respectively, and are calculated differently depending on whether the snow data comes from models or observations. For observed snow depth, u_{ρ_s} is described in the previous paragraph. For model snow depth, we use the SnowModel-LG outputs (Liston et al., 2020; Stroeve et al., 2020), processed with ERA-5 data, and u_{ρ_s} is derived from the difference between the snow densities provided by ERA-5 and MERRA-2, and similarly for the snow depth uncertainty (u_{h_s}). For observed snow depth, multiple products are utilized, including two climatologies for each hemisphere. For NH only: the merged AMSR-2 (Advanced Microwave Scanning Radiometer) and modified Warren99 (W99) climatologies (W99-AMSR2) as detailed in S. Paul et al. (2021). The W99 climatology from Warren et al. (1999) has been previously modified (divided by two) for first-year ice as introduced by N. T. Kurtz and Farrell (2011). The sea ice type information is taken from Copernicus Climate Change Service (C3S) Climate Data Record data set (CDR) and Interim Climate Data Record (ICDR) version v2 (Aaboe et al., 2021). Altimetric Snow Depth climatologies (ASD-clim) presented in Garnier et al. (2021) for both the Northern and Southern Hemisphere (NH & SH). In the Southern Hemisphere (SH), we additionally use the AMSR climatology (AMSR-clim) from the Sea Ice—Climate Change Initiative (SI-CCI) (S. Paul et al., 2021). Various snow depth products from radiometers are examined. These include snow depth data from SSMI/SSMIS (Special Sensor Microwave Imager and Special Sensor Microwave Imager Sounder) Markus and Cavalieri (2013) and J. Comiso et al. (2003) for both hemispheres (1991–2007 for SH and 1991–2017 for NH), and AMSR-E and AMSR-2 derived snow depth from the NASA National Snow and Ice Data Center (NSIDC) for both hemispheres (W. Meier, 2017). These gridded snow depth products provide daily estimates and so are averaged to obtain a monthly resolution.

For the weight estimation (w_k), the uncertainty (u_{h_s}) for climatologies, is the standard deviation of the snow depth per grid cell during the period considered for the climatology calculation. For AMSR and SSMI/SSMIS products, the uncertainty is the standard deviation per pixel of the snow depth within the month considered divided by the square root of the number of values used to compute the monthly mean.

Monthly snow depths are re-projected onto the Equal-Area Scalable Earth (EASE-2) grid with a resolution of 12.5 km using the Climate Data Operator (CDO) remap with the nearest neighbor option. Note that if there are two observations from the same type of instrument (e.g., SSMI and AMSR) in the same period, the weights are divided by two. In the following study, the weighted mean thickness SIT_{wm} is simplified and referred to as sea ice thickness (SIT) without further distinction, but it always refers to the weighted mean thickness.

2.2. Volume Estimation

Sea ice volume is calculated by integrating individual cell grid volumes of sea ice over the basin. To follow the ensemble approach of this study and to capture as much information as possible, the Climate Data Record (CDR) sea ice concentrations used for the period are the monthly OSISAF-(I)CDR (Ocean and Sea Ice Satellite Application Facility) (OSI SAF, 2022a; OSI SAF, 2022b) and NSIDC CDR sea ice concentrations (W. Meier et al., 2021). The two concentration products are considered equally likely and are therefore averaged with equal weight. This average is used as the concentration for the volume calculation. Individual volumes are integrated over the entire sea ice area A where the sea ice concentration is above 50% and on a specific mask, common to other products used in this study.

$$V = \int_A SIT_{SIC > 50\%} \cdot SIC_{SIC > 50\%} \cdot da \quad (4)$$

2.3. Uncertainty Quantification

Uncertainties in sea ice thickness are estimated using a stochastic approach with an ensemble of snow depth, snow density, sea ice density and radar freeboard estimates.

The radar freeboard ensemble is generated using a Monte Carlo approach. First, an ensemble of 10100 radar freeboard members is generated following Bocquet et al. (2023). The methodology has been adapted to generate spatially consistent members. In Bocquet et al. (2023), the radar freeboard members are generated randomly across the basin. This results in a spatially incoherent SIT for a given member and unrepresentative integrated volumes, but with a coherent individual grid cell distribution of radar freeboard. The generation of spatially consistent corrected radar freeboard was performed by decomposing and recomposing EOFs (Empirical Orthogonal Functions).

As presented above, the calibration procedure first consists of correcting Envisat over CryoSat-2 based on the sea ice surface state proxy. The parameters used for the regression are ice type fraction, sea ice concentration, leading edge slope and pulse peakiness of the waveforms, as well as the TFMRA50 LRM *FBr* (radar freeboard). These inputs are monthly grids with associated monthly uncertainties estimated during the data gridding process (Bocquet et al., 2023). In this study, the input and output ensemble (used to train an ensemble of 100 neural networks) for Envisat over CryoSat-2 is generated by performing a multivariate EOFs analysis using the Python package EOFs (Dawson, 2016) on the input uncertainties and a univariate on the CryoSat-2 radar freeboard uncertainties.

In fact, instead of generating completely random elements across the grid cells, the terms identified by the EOFs analysis are recombined, adding random noise to each term in the sum (see Equation 5). This method is commonly used to estimate the uncertainty of models and stochastic models Vervatis et al. (2016) and Ghantous et al. (2020). A spatially consistent noise map is generated and added to the inputs and outputs (Ω) of the neural networks to be trained. A noisy input Ω_i is obtained by adding noise Ω as: $\Omega_i = \Omega + \tilde{U}_{\Omega_i}$. In the previous study (Bocquet et al., 2023) $\tilde{U}_{\Omega_i} = U_{\Omega} \cdot \varepsilon_i$, where ε_i is a random number following a normal distribution centered on 0 with a standard deviation of 1, and U_{Ω} represents the uncertainty of the variables Ω . Here we have chosen to process the EOF decomposition on U'_{Ω} (U_{Ω} variability part). Ω_i can be calculated as follows:

$$\begin{aligned} U_{\Omega} &= \bar{U}_{\Omega} + U'_{\Omega} \\ U_{\Omega_i} &= \bar{U}_{\Omega} + \tilde{U}_{\Omega_i} \\ \tilde{U}_{\Omega_i} &= \sum_{j=1}^K E_j \cdot Z_j \cdot \varepsilon_{i,j} \end{aligned} \quad (5)$$

where E is the matrix containing the eigenvectors and Z the principal component vectors, i the member, j the modes and K the number of modes. $\varepsilon_{i,j}$ is the random value. A new one is chosen for each mode and each simulation, and re-initialized for each month. We assume that the uncertainty is not correlated from 1 month to another. Thus Ω_i depends on the spatial uncertainty but remains spatially consistent for each grid cell. This means that a low freeboard will not be found next to a grid cell with a very high freeboard unless it is captured by the initial signal. Note that $\varepsilon_{i,j}$ is spatially constant for 1 month and one mode. The first K modes are retained to explain 75% of the variance, corresponding to K = 48 for CryoSat-2 and K = 24 for Envisat. Based on this approach, an ensemble of 100 members of inputs is generated for Envisat and CryoSat-2. For each set of 100 members, 100 models are trained. These models are then applied to correct an ensemble of 100 TFMRA50 LRM noisy freeboards, also generated by reconstructing the signal with EOFs. This process results in 10,100 corrected Envisat radar freeboards for each month between 2002 and 2012. From the 10,100 Envisat corrected radar freeboards, 100 members are randomly selected for each month during the mission overlap period of Envisat and ERS-2 (2002–2003). An EOF decomposition is then performed to generate 100 grids of ERS-2 inputs, leading to the training of 100 additional models. Finally, this ensemble of models is used to correct ERS-2 and the same procedure is applied to ERS-1.

This approach results in the generation of an ensemble of 10100 monthly gridded radar freeboards for CryoSat-2 (and used to correct past missions), but also 10100 monthly gridded corrected radar freeboards for each legacy mission. Each of the 10100 radar freeboard grids is interpolated to fill the empty grid cells where the sea ice concentration is above 50%.

Once the ensemble of radar freeboards is generated, the next step is to generate an ensemble of each variable required to convert radar freeboard to sea ice thickness. An ensemble of snow depth products (with L members) available at the basin scale is then considered. Where available, for the Arctic: Snow-LG ERA5 (Liston et al., 2020), NASA Eulerian Snow On Sea Ice Model (NESOSIM) (v1. 1) (Petty et al., 2018), W99-AMSR2 climatology from SI-CCI, ASD-clim, for the Antarctic: AMSR-clim designed for SI-CCI, ASD-clim and snow depth derived from radiometry; SSMI/SSMIs, AMSR-E, and AMSR-2 (Cavalieri et al., 1996). Radiometry is not used in the case of the Arctic because spatial availability is not assured on Multi-Year Ice (MYI), preventing integrated volume calculation. When considering snow depth from observations, the snow density is randomly generated according to a Gaussian distribution with a standard deviation twice the uncertainty (u_{ρ_s}) centered on the snow density value (ρ_s), the value being spatially constant. The same procedure is used to obtain the ensemble of seawater and sea ice densities for Antarctica. Finally, the ensemble of Arctic sea ice densities is obtained by generating regression coefficients using the associated uncertainty from Jutilla et al. (2022).

The sea ice volume ensemble takes as input the $L * 10100$ SITs with two CDR concentration estimates (NSIDC and OSISAF) to compute $2 * L * 10100$ integrated volumes.

The ensemble approach provides a distribution of monthly SITs and volumes. Statistics on the ensemble allow us to quantify uncertainties. We perform percentiles, mean and standard deviation. The range presented in Figure 6 represents 90% of the values, corresponding to the 5th and 95th percentiles.

Figure A5 in the Appendix A, shows the effect of snow depth on sea ice volume for the product under consideration. For the Arctic, the figure highlights that the estimates from this time series are overestimated compared to SI-CCI (Paul et al., 2018, 2021) and CS2SMOS (Soil Moisture and Ocean Salinity/CryoSat-2 merged product) (Ricker et al., 2018), mainly due to the chosen sea ice density parameterization from Jutilla et al. (2022). Figures A1 and A2 present statistics on the sea ice thickness ensemble, focusing on percentiles as well as mean and standard deviation for each mission and during each mission overlap period.

2.4. Thickness and Volume Evaluation

The SIT time series is reliant on altimetry-based radar freeboard with an ensemble of different snow depths (as explained in Section 2.1). As some of the independent data sets used for comparison only provide draft or total freeboard, and we do not have derived snow thickness from our weight-averaged SIT, we calculated weight-averaged draft and weight-averaged total freeboard as for thickness to ensure comparable measurements.

Thickness and volume are validated using in situ data, airborne data and other satellite-based SIT measurements. Except for fixed moorings and airborne campaigns, satellite sea ice thicknesses are re-gridded with CDO on the EASE-2 12.5 km grid.

A challenge in this comparison is to assess whether the long-term evolution of sea ice thickness is accurately captured by the altimeters. However, there are few long-term in situ records available for both hemispheres. In addition, comparing estimates from different sensors involves resolving issues related to different time and space scales.

2.4.1. Arctic Sea Ice Thickness Validation

In the Arctic, 8 moorings from 2 different projects have been maintained for several decades in two regions. The Beaufort Gyre Experiment Project (BGEP), operated by the Woods Hole Oceanographic Institution (WHOI), is located in the Beaufort Gyre. In addition, moorings in Fram Strait are managed by the Norwegian Polar Institute (NPI) (Sumata et al., 2023). Data from the BGEP moorings consist of daily estimates of sea ice extent. For ease of interpretation, a 31-day rolling mean is applied. For comparison with the monthly sea ice draft time series, the mooring locations are matched to the corresponding grid cells. The NPI sea ice drafts are distributed as monthly estimates; the comparison is made with the corresponding grid cell satellite sea ice drafts. In order to better capture past evolution, sea ice drafts from US Navy and Royal Navy submarine cruises have been included in the

comparison (National Snow and Ice Data Center (Comp.), 1998; Rothrock et al., 1999). These cruises, which took place mainly at the end of the 20th century and occasionally after 2000, provide extensive spatial coverage as they typically crossed the Arctic Ocean.

2.4.2. Antarctic Sea Ice Thickness Validation

For the Antarctic, the ASPeCt (Antarctic Sea Ice Processes & Climate) program provides ship-based estimates of sea ice thickness for over 40 years (Kern, 2020; Worby et al., 2008). ASPeCt data are processed to obtain total thickness (level plus ridged ice) as described in Worby et al. (2008). All estimates of effective thickness are combined into monthly grids and compared with the monthly estimates from the time series. A limitation of this data set is that ship-based thickness observations may be biased low due to under-sampling of thick ice, as icebreakers tend to follow routes through thinner ice (Kern et al., 2016; Worby et al., 2008). The Alfred Wegener Institute (AWI) provides some sea ice drafts from moorings (Behrendt et al., 2013), providing estimates mainly on the 0°E meridian and in the western part of the Weddell Sea. AWI moorings are processed similarly to BGEF moorings. Given the sparse validation data available for the Antarctic, we have included two Operation IceBridge (OIB) (N. Kurtz et al., 2015) campaigns in 2009 and 2010 in the Weddell Sea and Bellingshausen Sea to add confidence to the retrieval, as these two regions have the highest discrepancies with ASPeCt. The Operation IceBridge (OIB) campaigns used here provide total freeboard measurements, including both snow depth and ice freeboard. The monthly weighted total freeboard is projected along the OIB ground tracks for comparison. Radar freeboards are also shown to illustrate whether the radar pulse reaches the snow or the sea ice surface, compared to the Operation IceBridge (OIB) data.

2.4.3. Arctic and Antarctic Volume Validation

Sea ice volumes are also compared with outputs from several models: The Pan-Arctic Ice Ocean Modeling and Assimilation System (PIOMAS) for NH and the Global Ice Ocean Modeling and Assimilation System (GIO-MAS) for SH (Zhang & Rothrock, 2003), OPA-NextSim (NH) (Boutin et al., 2023). These estimates are compared with SI-CCI v2.0 products, sea ice volumes derived from Envisat (Hendricks et al., 2018b, 2018d) and CryoSat-2 (Hendricks et al., 2018a, 2018c), and the CS2SMOS monthly volume derived from the merged CryoSat-2 and SMOS thickness product. We also compare the volume estimates with the ensemble mean of the Coupled Model Intercomparison Project Phase 6 (CMIP6) models, in particular the Ocean Model Intercomparison Project Phase 2 (OMIP-2) simulations, with the JRA-55 reanalysis. The models used to compute the ensemble mean monthly sea ice thickness and volume include NorESM2, MRI-ESM2, EC-Earth3, CNRM-CM6, CMCC-CM2, and MIROC6. Note that sea ice volumes are computed for each data set taking into account the orbit constraint at 81.5°N and the sea ice concentration threshold of 50%.

2.5. Trend Estimation

Trends are analyzed using the Theil-Sen estimator (Sen, 1968; Theil, 1950). The trend is associated with uncertainties equal to the uncertainty due to the regression (not the estimation), with a 90% confidence interval and a Mann-Kendall test of statistical significance (Kendall, 1948; Mann, 1945).

3. Homogeneous Sea Ice Thickness Records 1994–2023

Arctic and Antarctic sea ice are undergoing significant changes in thickness. While the Arctic is becoming thinner over most of the basin, thickness trends in the Antarctic vary considerably from region to region. Figure 1 illustrates the changes in ice thickness in each region and throughout the year.

Sea ice thickness trends in the central Arctic seas, when statistically significant, are negative for all winter months. The East Siberian and Chuckchi Seas are particularly affected by sea ice thinning, with trends ranging from 10 to 30 cm/decade. In the Barents and Kara Seas, thinning occurs mainly in late winter (February–April), up to 15 cm/decade. In general, the beginning of winter is more affected by thinning than April, which can be partly explained by the later melt onset (Stammerjohn et al., 2012). The Beaufort Sea doesn't seem to be affected by changes in thickness, which can be explained by a multi-year loss of thick ice from the central Arctic passing through the Beaufort Gyre. Thickening of this ice is observed in the East Greenland Sea, while moorings indicate that sea ice in Fram Strait is thinning (Sumata et al., 2023). In this region, the snow depth is increasing (Zhou et al., 2021) and

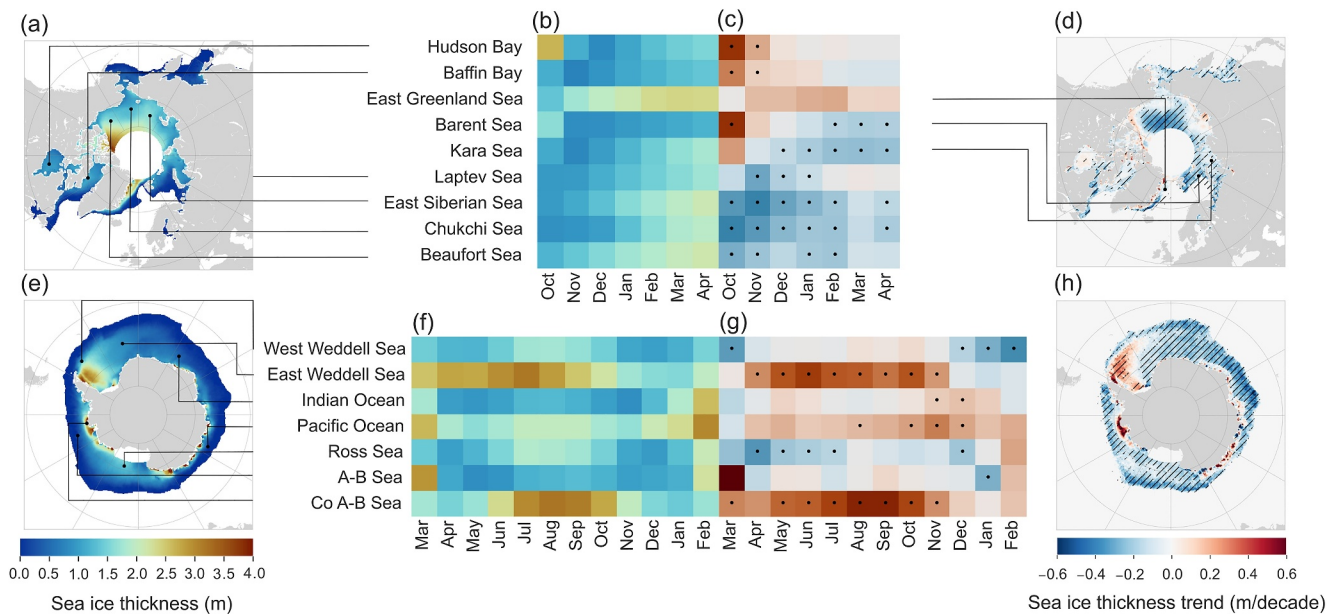


Figure 1. Sea ice thickness trends in the Arctic and Antarctic. (a) Arctic and (e) Antarctic mean sea ice thickness over the period 1994–2023. (b) Arctic and (f) Antarctic mean sea ice thickness for each region (y-axis) and for each month (x-axis) over the period 1994–2023. Panels (d and g) are similar to (b) and (f) respectively, but show the thickness trends. Black dots enhance trends with $(1 - p\text{-value}) > 0.95$. Panels (d and h) are sea ice thickness trends over the period 1994–2023.

the modeled snow density is higher (Stroeve et al., 2020) than in other regions, which may explain a potentially inaccurate positive trend in thickness (see Figure A3).

The evolution of Antarctic sea ice thickness also shows significant trends over the past 30 years, comprising both positive and negative changes, with pronounced regional differences. In particular, thickening trends of about 30 cm/decade are observed in the western part of the Weddell Sea and the coastal regions of the Amundsen and Bellingshausen Seas. These trends are also reflected in the models for the first two decades (Holland et al., 2014; Massonnet et al., 2013). In the Indian Ocean sector, a more pronounced thinning trend is observed in winter, with sea ice thinning at a rate of about 20 cm/decade in September, corresponding to a total thinning of 60 cm over the 30-year period. However, this thinning is offset by the thickening of coastal ice within the region. In the Ross Sea, sea ice thinning occurs during the freeze-up season, with a thinning rate of about 15 cm/decade, possibly related to increasing sea ice drift (Haumann et al., 2014; Holland & Kimura, 2016).

4. Thickness Validation

Lack of in situ data sets makes thickness validation challenging, especially for long-term time series.

4.1. Arctic Sea Ice Thickness

For the Arctic, we compared the sea ice draft of each mission with 8 different moorings, four in the Beaufort Sea (BGEP) and four in Fram Strait (NPI). In the Beaufort Sea (Figure 2), the thickness evolution over winter is well represented, but suggests that the draft is slightly overestimated, especially for the CryoSat-2 period (by about 20 cm). The Fram Strait moorings capture the same feature (Figure 3), showing an overestimation of Cryosat-2 SIT but an underestimation of ERS-1 and ERS-2, with an overall positive bias of 10 cm across the four stations. Translating this result into trends would result in an underestimation (of the negative trend) in these regions compared to the moorings. We also consider data from the NSIDC's Submarine Upward Looking Sonar Sea Ice Draft, which crossed the Arctic Ocean. With respect to satellite flight periods, sea ice drafts derived from altimetry are compared to the Scientific Ice Expedition (SCICEX) campaigns of 1996, 1997, 1998, and 1999, as well as three other cruises: one in 2002 and two in 2005 (Figure 3). Satellite-based drafts are biased by 11 cm (Envisat) to 16 cm (ERS-2), but the correlation between drafts remains high, especially for ERS-2. These correlations, considering the number of points, indicate that for the late 1990s and early 2000s the observed trend is consistent with the submarine observations.

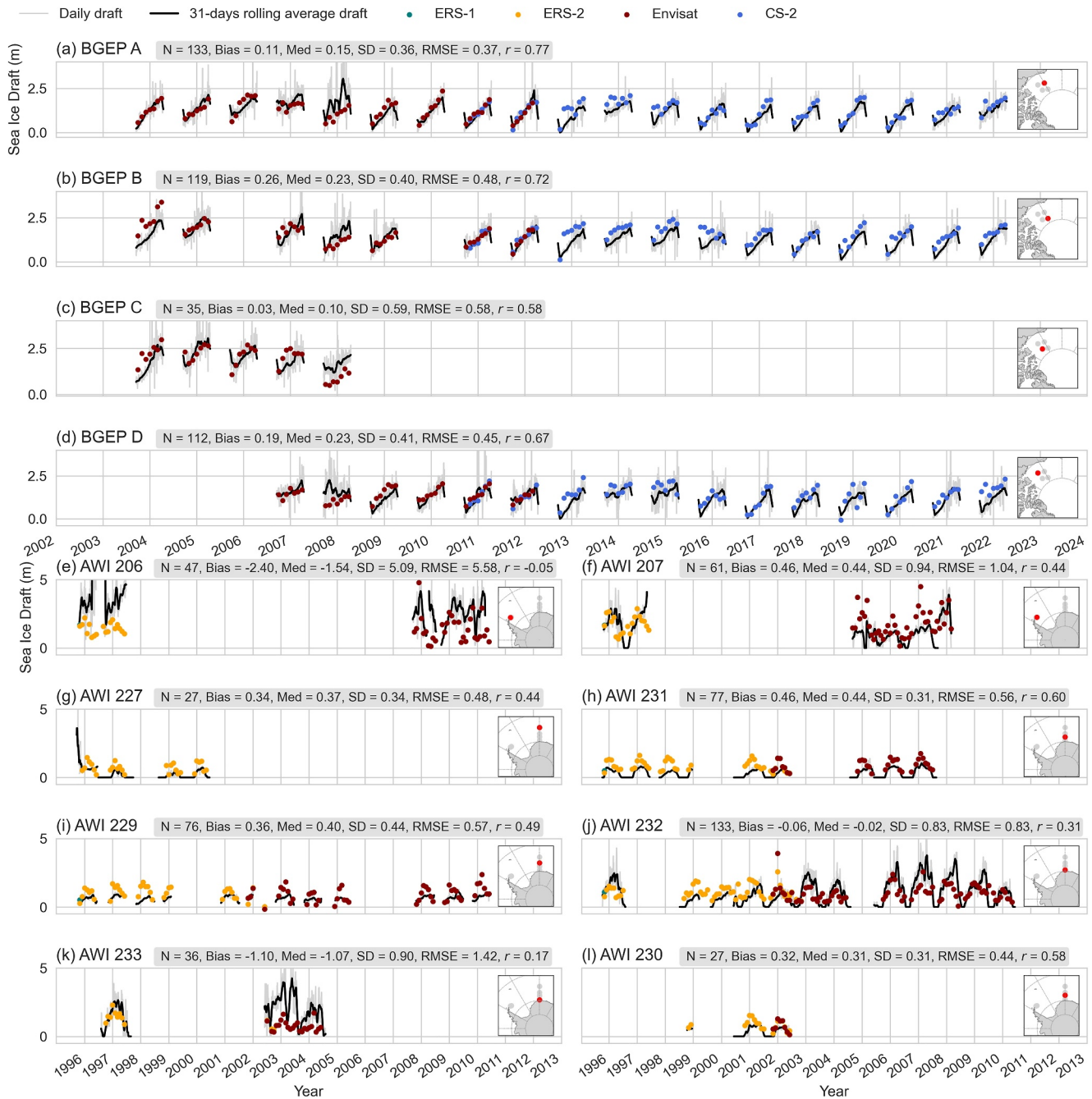


Figure 2. Comparison of Arctic sea ice drafts at BGEP moorings in the Beaufort Sea (NH) (a–d) and at AWI moorings in the Weddell Sea (SH) (e–l). Altimeter-based sea ice drafts (colored dots), daily sea ice drafts in gray, and monthly rolling averages in black. Red dots correspond to Envisat, blue to CryoSat-2, orange to ERS-2 and teal to ERS-1. Statistics correspond to (satellite moorings).

4.2. Antarctic Sea Ice Thickness

For the Antarctic, we consider the ASPeCt data set (Figure 4), which compiles ship-based estimates of sea ice thickness over the period considered. A global overestimation of thickness is observed, especially in the Weddell and Ross Seas. The thickness of the Pacific sector is well captured, but shows an underestimation in the late period (2003–2019).

Comparisons of total freeboard with OIB campaigns (Figure 5) in October 2009 and 2010 reveal good agreement and the spatial evolution is well captured. OIB total freeboards are within the uncertainty range of Envisat and

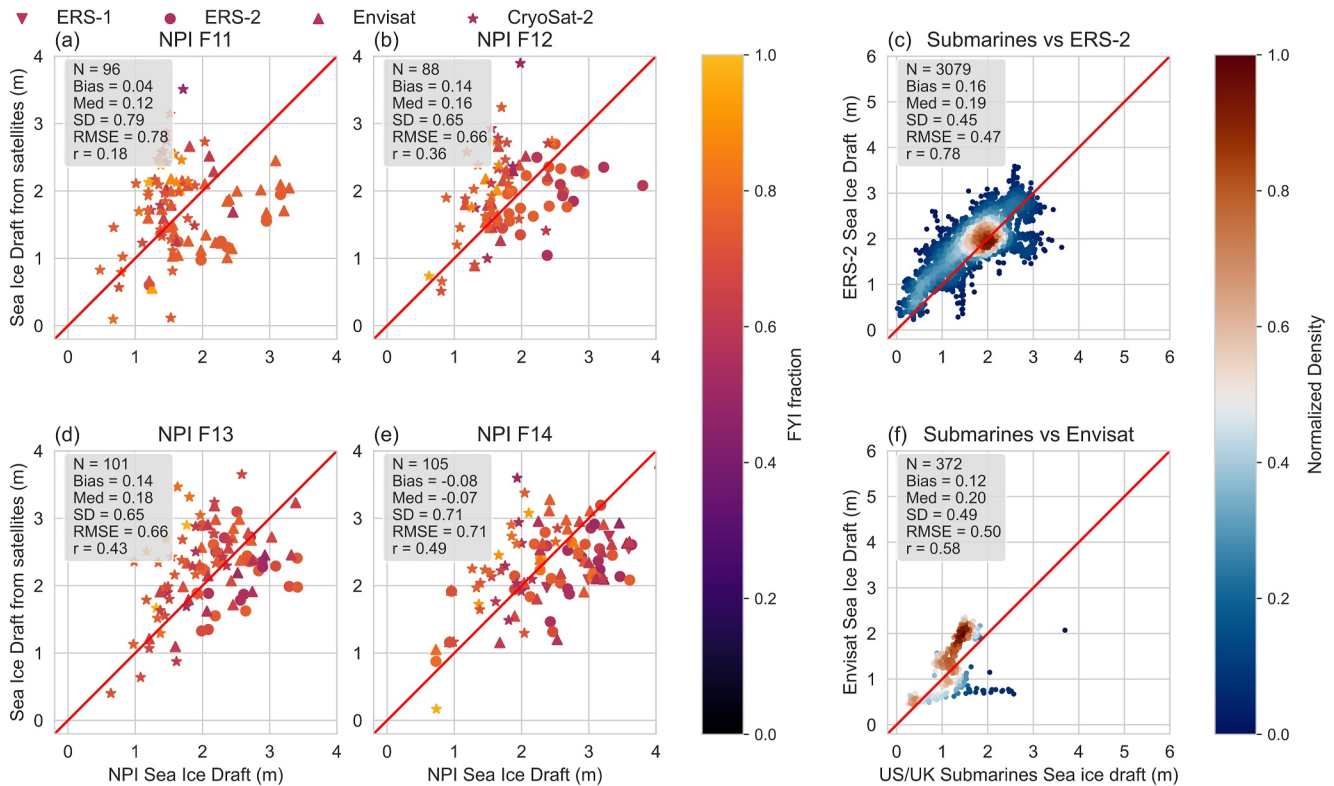


Figure 3. Comparison of NPI Arctic sea ice drafts in Fram Strait, UK/US Navy submarine sea ice drafts, and altimetry-based sea ice drafts. Altimetry-based sea ice drafts are a function of NPI sea ice drafts. (a) Corresponds to F11, (b) F12, (d) F13, and (e) F14. Statistics correspond to (satellite moorings). Panel (c) shows comparison between ERS-2 and sea-ice draft submarines and (f) the same for Envisat sea-ice draft.

CryoSat-2 for 5 out of 6 campaigns. However, this comparison only assesses the agreement between total freeboards and does not consider sea ice thickness. Consequently, assumptions about sea ice density are not taken into account, nor is the contribution of snow and ice to the total freeboard measurements. Nevertheless, it is important to note the consistency in both the spatial evolution and the magnitude of the total freeboard. Figure 5 also illustrates the radar freeboard computed for the time series. The radar freeboard values are slightly lower than the OIB total freeboard, suggesting that the radar altimeter measurement at least partially penetrates the snow layer.

Moorings in the Weddell Sea sector (Figure 2) show an underestimation of draft along the coast (AWI 230–233) and an overestimation near the sea ice edge (AWI 227–229). Seasonal variability is generally well represented. Thick ice in the western Weddell Sea sector (AWI 206, AWI 207) is underestimated compared to one mooring and overestimated compared to the other. For the longest record of this mooring, ERS-2 appears to overestimate draft while Envisat underestimates it, possibly leading to an overestimation of the negative trend in thickness in this region.

Validation of long-term records is challenging in both hemispheres because of the limited availability of long-term in situ records, which are primarily collected at very localized locations, such as moorings, or by different methods, such as visual ship-based observations. Local drafts are averaged and compared to monthly mean conditions. Comparison with ASPeCt, for example, remains a challenge. Some of the values are less accurate (visual estimates), and we tend to compare estimates from a specific location and time to an average estimate of thickness over a month. Regions observed by Operation IceBridge (OIB), such as the Amundsen and Bellingshausen coastal areas, often have low sea ice drift, resulting in more stable sea ice thickness conditions. Similarly, the coastal Weddell Sea tends to have relatively stable sea ice thickness compared to other regions. Although ASPeCt data are averages, sea ice changes rapidly in most Antarctic regions, making it challenging to obtain monthly state measurements. In regions such as Weddell and A-B, where the ice is thicker, the distribution of thick ice may be under-sampled. There remains a significant gap between in situ observations and satellite retrievals, making it difficult to draw definitive conclusions. Although thickness and volume may appear to be

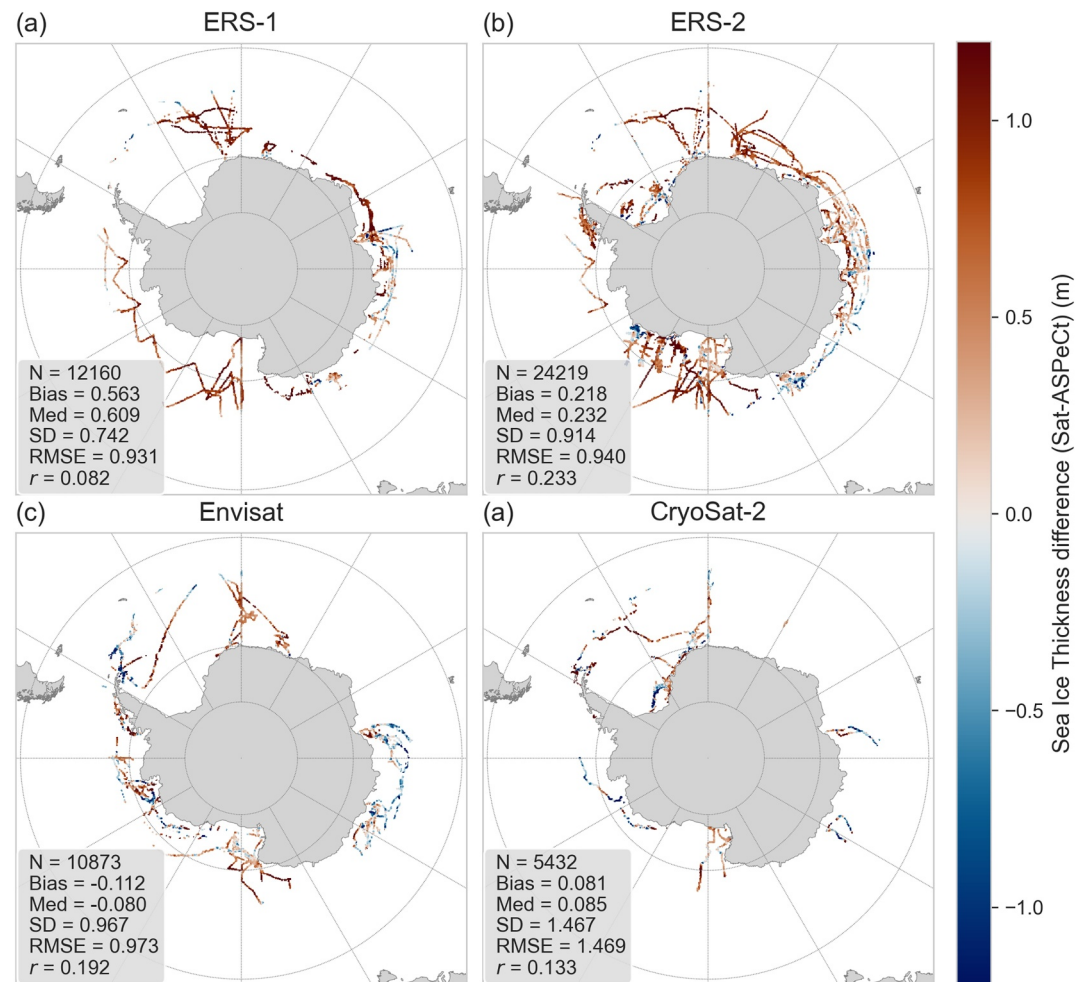


Figure 4. Comparison of Antarctic sea ice thickness with ASPeCt. Sea ice thickness from ERS-1 (a), ERS-2 (b), Envisat (c) and CryoSat-2 (d) with ASPeCt sea ice thickness for Antarctic sea ice. Statistics correspond to (Satellite-ASPeCt).

overestimated compared to models for the Southern Ocean, comparisons indicate that the overall freeboard magnitude is well captured and that draft may be overestimated in some winters and underestimated in others. ASPeCt shows a global overestimation compared to satellite data, as also found by Fons et al. (2023).

Furthermore, the spatial and temporal evolution of sea ice thickness seems to be well captured by the altimeter-based retrievals. However, a potential underestimation of the negative trend in sea ice thickness is observed in the Beaufort Sea.

Figures A3 and A4 refer to sea ice thickness estimates using several snow depth products (both models and climatologies). These figures highlight the value of examining a combined time series of sea ice thickness from different snow depth products. Validation statistics against moorings show better agreement with weighted means of sea ice thickness, regardless of hemisphere. It is also observed that the variability of sea ice thickness derived from the weighted mean is higher over the 30-year period compared to sea ice thickness estimates from snow depth climatologies. In addition, for the Antarctic, the weighted mean sea ice thickness falls between the other sea ice thickness estimates computed using climatologies. In the Arctic Ocean, the assessment is similar, except for the marginal ice zone in the Atlantic sector (Greenland Sea).

5. Sea Ice Volume Between 1994 and 2023

Monthly sea ice volume is calculated by integrating sea ice thickness and concentration within each basin. Sea ice concentration estimates are derived and averaged from both the NSIDC-CDR and OSISAF-CDR data sets. To

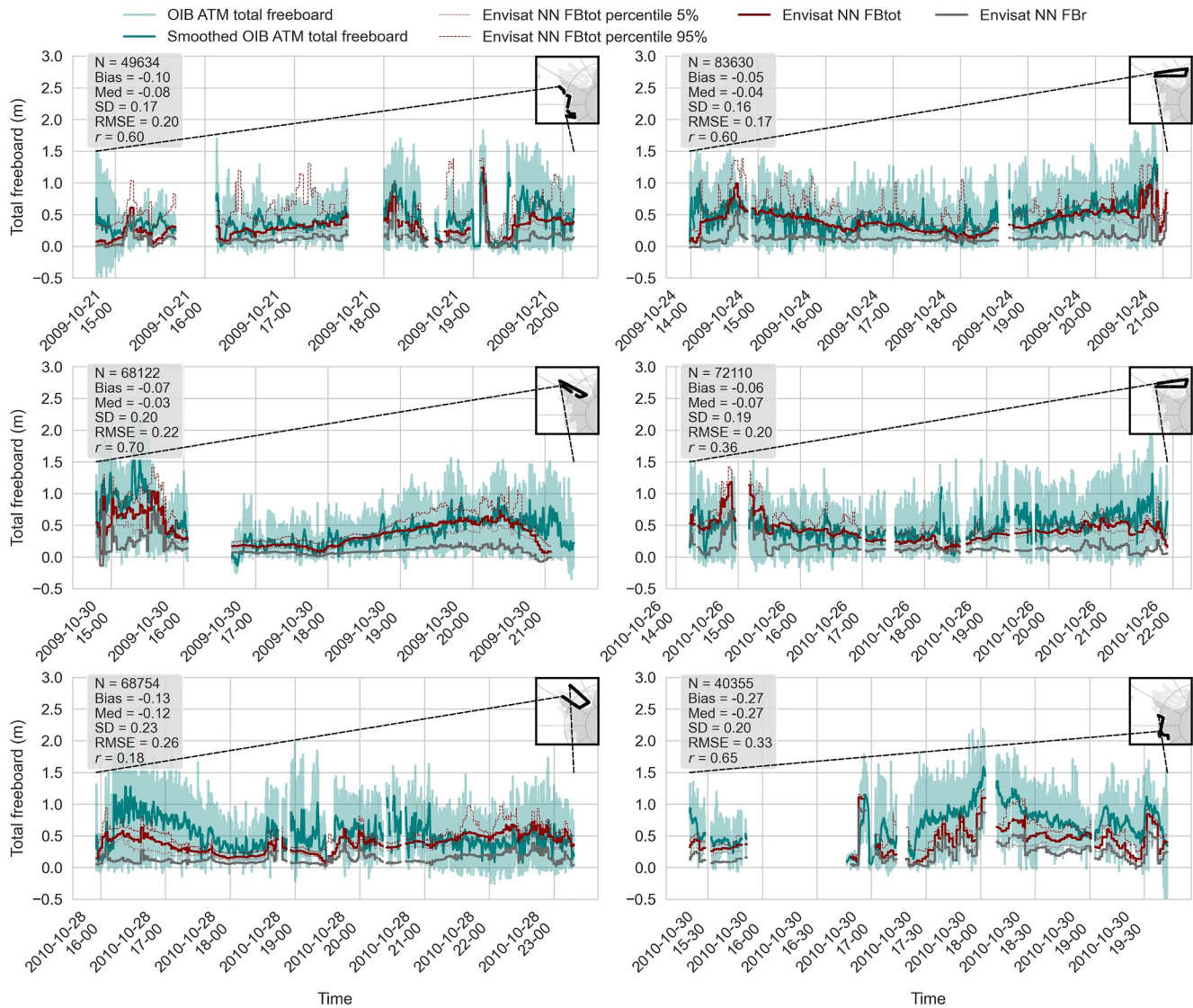


Figure 5. Comparison of Antarctic total freeboard (sea ice freeboard + snow depth) between Envisat estimates and OIB along the ground track of six missions in the Weddell and Bellingshausen Seas for 2009 and 2010. Altimeter-based total freeboard (Envisat NN FBtot) in red and radar freeboard in dark. Operation Ice Bridge (OIB) total freeboard smoothed and raw measurements. Red dashed lines are the percentiles at 5% and 95% of total freeboard.

ensure comparability, volumes are integrated using a common mask applied to all sea ice thickness products, including both models and observations. This integration considers only positive sea ice thickness values and includes a minimum sea ice concentration of 50%.

Arctic sea ice volume up to 81.5°N shows a consistent decrease during all winter months (October–April). The most pronounced decline occurs in October, with a decrease of $-144.9 \pm 55.84 \text{ km}^3/\text{year}$, while the least pronounced decline occurs in March, with a decrease of $-83.15 \pm 34.75 \text{ km}^3/\text{year}$. Sea ice volume is less affected in late winter due to a delay in sea ice thickening. The seasonal cycle is well captured by PIOMAS, OPA-NextSim, and the OMIP-2 ensemble mean (Figure 6). However, the sea ice volume estimates are consistently biased high compared to the CCI estimates, primarily due to differences in sea ice density. All estimates are within uncertainty bounds and within the range of inter-annual variability. Regionally, sea ice volume is decreasing in all areas except Hudson Bay and Baffin Bay. The three Siberian seas show a turning point in 2006 (for the period 1994–2023), where positive anomalies turned negative without returning to previous states. No significant trend in global Antarctic sea ice volume is observed, except for a significant volume loss in 2016. This finding is

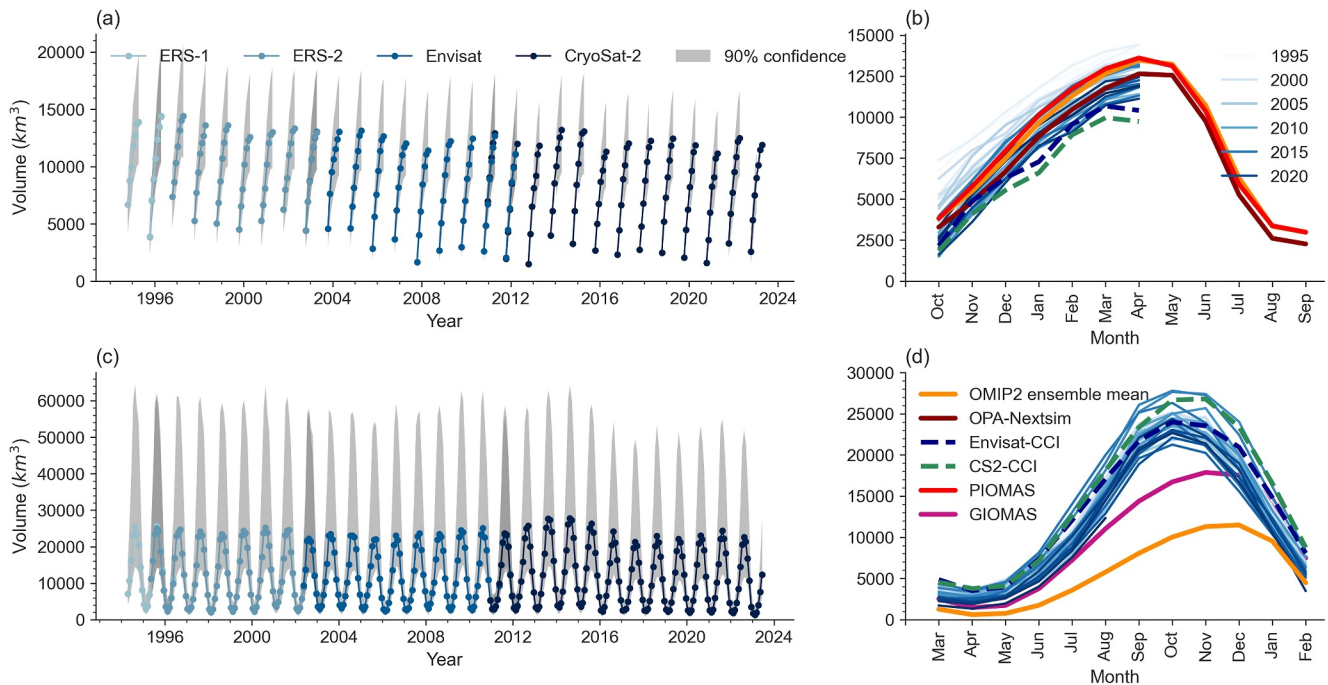


Figure 6. Sea ice volume (where sea ice concentration is above 50%) for NH, restricted to 81.5°N (a, b) and SH (c, d), from observations and models. Blue shading for the four missions. Panels (b and d) show the volume for each winter (for the time series presented in this paper) and seasonal cycle for Envisat-CCI (2003–2012), CryoSat-2-CCI (2010–2017), OMIP2 (1990–2018) ensemble mean volume and PIOMAS (1990–2020), OPA-NextSIM (2000–2018) for NH and GIOMAS (1990–2020) for SH.

consistent with previous studies (Fons et al., 2023; Garnier et al., 2022) and sea ice extent records (Purich & Doddridge, 2023).

The magnitude of Antarctic sea ice volume presented in this study is in good agreement with the SI-CCI estimates. However, when compared to GIOMAS and the OMIP-2 ensemble mean, our observations show a higher bias, with volumes almost twice as large as those predicted by the models. In addition, the duration of sea ice advance is longer in the models compared to the observations, and while the onset of sea ice retreat is observed in September, the models indicate that it occurs in October (Figure 6).

Regionally, decreases in sea ice volume in 2016 are observed in the East Weddell Sea, the Indian Ocean sector, and the Ross Sea sector (Figure B3). The Amundsen-Bellingshausen Sea shows no significant changes, except for an increase in volume after 2016. The western part of the Weddell Sea shows a similar trend with ice thickening.

Figures A5 highlights the significant impact of various snow depth products on sea ice volume estimates, particularly in the Arctic sea ice volume trends shown in Table A1. The trends differ substantially depending on the type of snow depth product, especially at the end of winter, with differences by a factor of 2–3 when comparing Snow-LG with ASD-clim. Although the discrepancies between the trends are smaller in October, sea ice volumes calculated using modeled snow depth still show higher negative trends.

6. Sea Ice Volume Variability: Attribution to Thickness Variability

Sea ice volume, like any geophysical field, can be decomposed into a sum of a mean term \bar{V} (representing the seasonal cycle) and a variable term V' , which denotes the volume anomaly. Similarly, this decomposition can be applied to SIC and SIT, resulting in the volume anomaly (V') being explained in terms of sea ice thickness variability (SIT') and sea ice concentration variability (SIC') relative to their respective seasonal cycles (\bar{SIT} and \bar{SIC}), see Equation 6. Volumes are integrated for each grid cell of area da over the entire basin of area A .

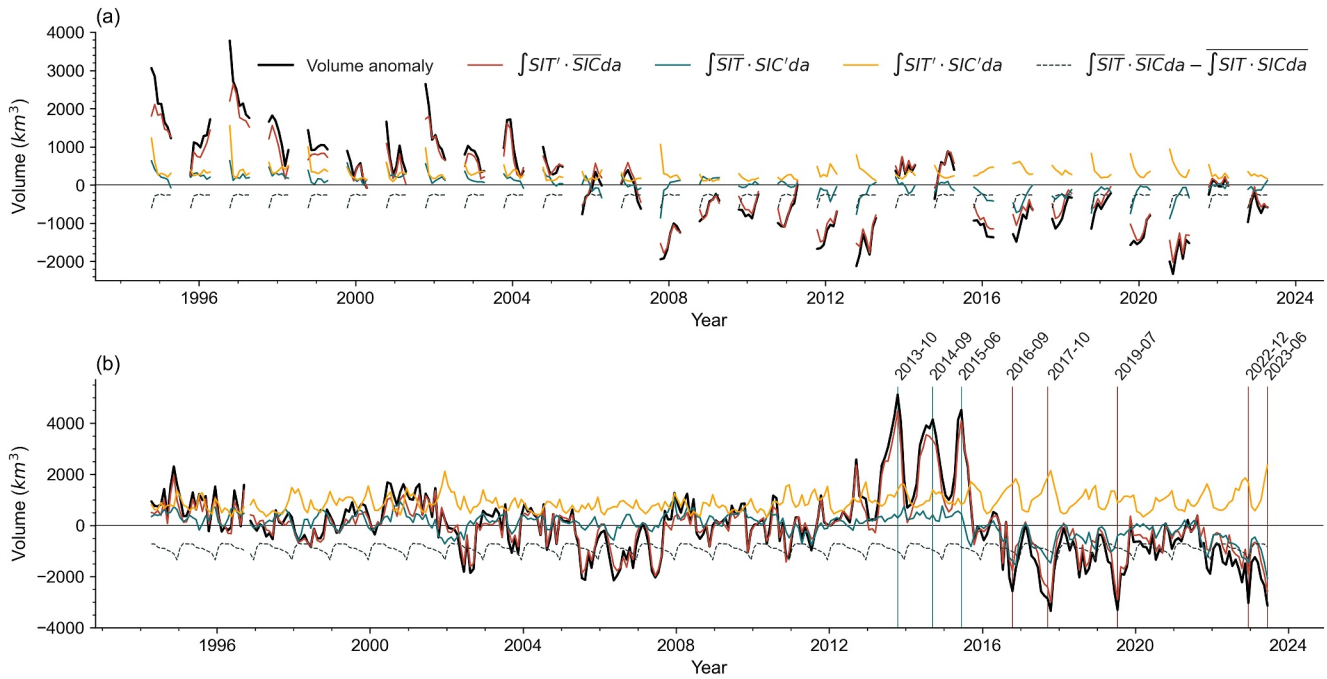


Figure 7. Sea ice volume anomaly (1994–2023) decomposed into thickness variability and concentration variability. (a) For Arctic sea ice and (b) for Antarctic sea ice.

$$\begin{aligned}
 V &= V' + \bar{V} \\
 V' &= V - \bar{V} \\
 V' &= \int_A SIT \cdot SIC - \overline{\int_A SIT \cdot SIC \cdot da} \\
 V' &= \int_A SIT' \cdot \overline{SIC} \cdot da + \int_A \overline{SIT} \cdot SIC' \cdot da + \int_A SIT' \cdot SIC' \cdot da + \int_A \overline{SIT} \cdot \overline{SIC} \cdot da \\
 &\quad - \overline{\int_A SIT \cdot SIC \cdot da}
 \end{aligned} \tag{6}$$

For both hemispheres, sea ice thickness variability explains more than 95% of volume variability (Section 7). Conversely, sea ice concentration variability explains 53% for NH and 42% for SH of sea ice volume variability, with both terms being correlated. The correlation values between SIT and SIV variability are higher in winter than in summer.

The variability of Antarctic sea ice volume during the 4 years before and after the 2016 drop is even more dominated by thickness variability. The three minima of sea ice area anomalies were recorded in December 2016, January 2023, and June 2023 (Purich & Doddridge, 2023), while the minima of sea ice volume anomalies occurred in October 2017, July 2019, and June 2023 (Figure 7). Regarding the covariance term $SIT' \cdot SIC'$, there is a clear change in the annual evolution starting in 2011. Prior to 2011, the covariance term mainly reflected noise, but since then a distinct seasonal variation has emerged. Higher covariance terms are observed during winter and lower during the melt season. This suggests that although volume variability is still dominated by thickness variability, sea ice concentration anomalies and sea ice thickness anomalies show similar extreme patterns during winter. Notably, the positive Antarctic anomalies of 2014 and 2015 also correspond to the last two positive anomalies observed in the Arctic.

Looking at the anomalies, we can note that the eastern part of the Weddell Sea has an interesting 8-year cycle.

Since volume variability is explained by thickness variability, the following idea is to identify regime changes in sea ice thickness within volume changes.

Figure 8 illustrates how sea ice thickness contributes to volume in terms of thickness categories. In the Arctic, despite the observed decline in sea ice volume and thinning trends, the proportion of thick ice in the total volume has remained relatively stable over time. This stability is partly due to data coverage limitations beyond 81.5°N, which excludes most of the MYI. In particular, the winters of 2007–2008 and 2012–2013 experienced significant summer volume loss due to substantial MYI export (Kwok et al., 2009). These winters started with low ice extent and predominantly thin ice, which then thickened over time. In March of these years, 75% of the volume consisted of ice thinner than 2 m. The period between 2013 and 2015 saw a marked increase in volume due to thickening ice (R. Tilling et al., 2015), with 60% of the volume attributed to ice thicker than 2 m. This thickening phase was followed by a volume loss during the winter of 2015–2016 (Ricker et al., 2017).

In the Southern Ocean, we observe a significant increase in volume from 2012 for the months of May–November. This increase is primarily attributed to significant ice thickening during these months. The proportion of the total volume accounted for by ice thicknesses greater than 3 m increased from 20% in 2002 to 40% in 2013. The year 2016 marks a regime shift in terms of concentration, extent (Purich & Doddridge, 2023) and, most importantly, sea ice volume. Despite an overall decrease in sea ice volume for each month after 2016, the volume of ice thicker than 3 m, while decreasing, stabilized at about twice the level of years before 2016. In summary, as noted in the previous section, ice thickness increased in certain regions from 2012 onward, resulting in a larger proportion of total volume. This trend of increasing thickness continued, contributing to the stabilization of the overall volume after the decline observed in 2016.

7. Discussion and Conclusions

This study presents the first homogeneous 30-year (1994–2023) time series of sea ice thickness and volume for both polar oceans. These time series represent a significant advance in long-term observations of sea ice thickness. To ensure consistency, the time series are based on CS-2 sea ice thickness data (using the TFMRA50 retracker). Legacy missions have been adjusted sequentially, with each older mission adjusted to the most recent. The conversion from radar freeboard to snow depth is achieved by incorporating a set of snow depth products, leveraging the strengths of each over the 30-year period. Uncertainties are estimated using a stochastic approach.

In addition, the study uses a new parameterization of Arctic ice density as a function of ice freeboard (Jutilla et al., 2022), adapted to the long series. However, this increases the thickness and therefore volume compared to the traditionally used ice-type-based parameterization, which explains the overestimation of volume compared to SI-CCI (Paul et al., 2018, 2021).

Comparisons with independent data sets suggest a potential overestimation of ice thickness by CryoSat-2 and an underestimation by ERS-2 and ERS-1 (NH), which may indicate an underestimation of negative trends. However, drawing conclusions about Antarctic sea ice thickness is challenging due to low data availability and higher sea ice export compared to the Arctic. The spatial evolution of thickness in October over 2 years is well represented in the Weddell and Bellingshausen Seas, where the largest differences with ASPeCt data are observed. In the near future, more independent data sets are needed to validate future trends and sea ice thickness records, but along with different measurement techniques to account for scale differences between satellite and in situ measurements.

Notable discrepancies between model predictions and observations in Antarctica require further investigation. Both estimates are potentially biased: models may fail to represent total sea ice growth as well as significant dynamically induced growth, whereas altimetry-based measurements may be biased by snow or sea ice surface conditions.

Theoretically, snow-ice formation and flooding pose a significant challenge in estimating sea ice thickness in the Antarctic. However, when considering satellite estimates of both snow depth and sea ice thickness, the impact is minimal because the densities of snow ice and sea ice are similar. Even when the estimated snow depth is underestimated and the remaining snow depth is included in the sea ice freeboard, the approximation of sea ice thickness remains relatively accurate. In other words, the biases cancel each other out, even though individual estimates may not be accurate independently. However, this could have implications for the freshwater budget, as ice is not formed by the same processes.

The limitations of this study, including the penetration of the signal within the snow cover and flooding, are considered in the uncertainty budget. In addition, we avoid choosing a specific snow depth product for the time

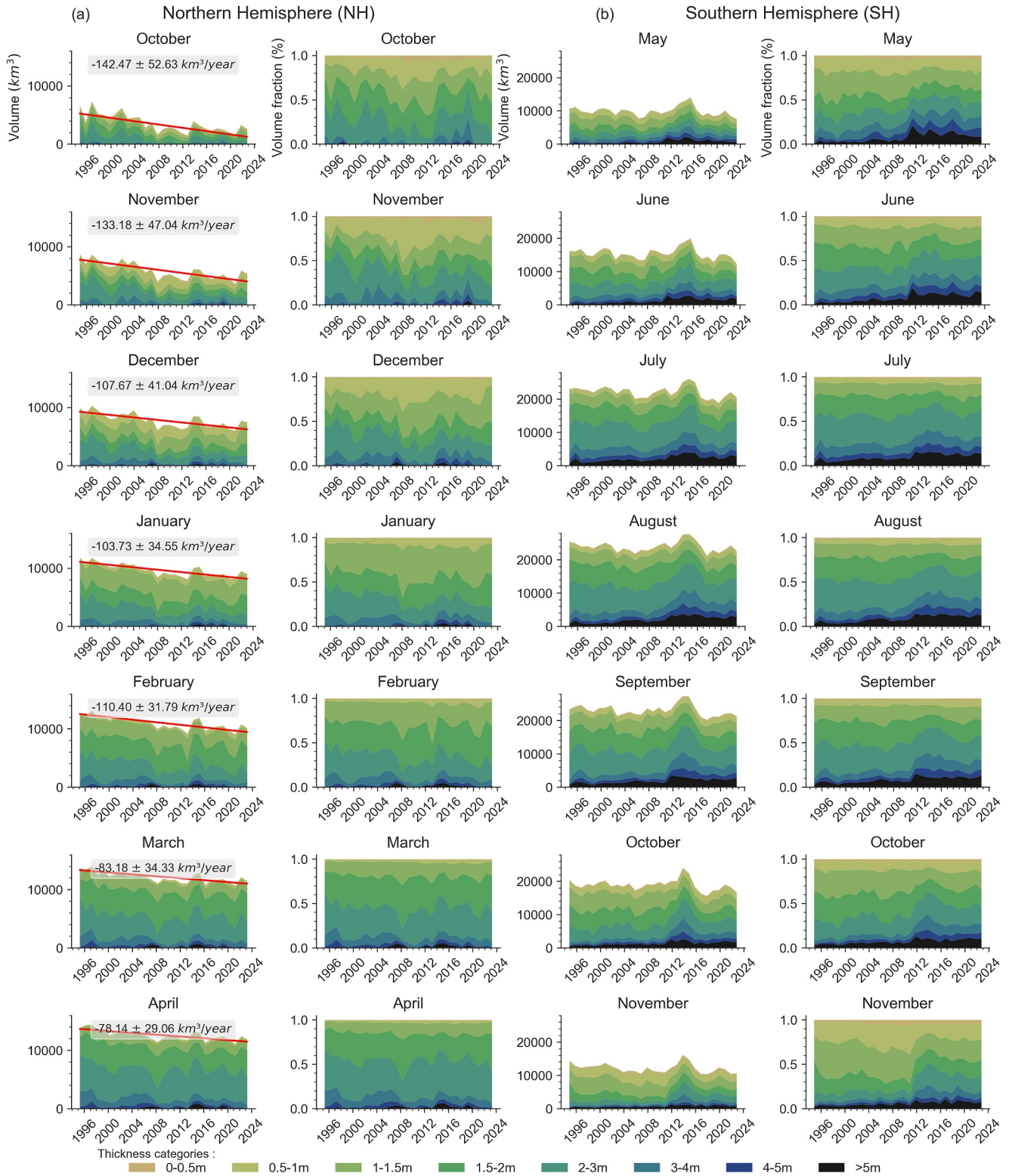


Figure 8. Sea ice volume for each winter month and each sea ice thickness category. Trends are shown for sea ice volume for each month, with the uncertainty from the trend estimate. All trends are statistically significant with $(1 - p\text{-value}) > 0.95$.

series by using weighted averages of snow depths from multiple sources, taking into account the uncertainty of snow on sea ice thickness.

In contrast to previous studies such as SI-CCI (Paul et al., 2018, 2021), this analysis also includes the temporal evolution of snow depth on sea ice. Our results show a consistent negative trend in Arctic sea ice volume during all winter months (1994–2023), confirming the ongoing thinning of the ice and characterizing monthly regional changes. In the Antarctic, we observed complex and spatially heterogeneous changes. Significant trends are identified, including thickening in the Weddell Sea and along the coast of the Amundsen-Bellinghshausen Sea. This homogeneous time series is likely to address the need for long-term thickness data highlighted in several publications (Haumann et al., 2016; M. Meredith et al., 2019). We confirmed that the volume of Arctic sea ice has decreased significantly in the last 30 years, reflecting a widespread thinning of the ice. In contrast, there is no trend in global sea ice volume for the Antarctic, which can be attributed to recent fluctuations, in particular an increase in 2011 followed by a sudden decrease in 2016. We emphasize that changes in sea ice volume are predominantly (95%) explained by variations in thickness. Investigating changes in sea ice thickness regimes can provide valuable insights into changes in volume.

Finally, the time series, combined with their uncertainties, provide a robust data set from which to analyze the various changes in sea ice over the past 30 years (1994–2023) from new knowledge and a variety of climate studies.

Appendix A: Ensemble Statistics for Sea Ice Thickness Uncertainty Characterization and Impact of the Snow Depth Product on Sea Ice Thickness and Sea Ice Volume

Figures A1 and A2 present the statistics of the ensemble of sea ice thickness during a winter month used for the uncertainty quantification. Figures A3 and A4 show the effect of the estimate of snow depth on the thickness of the sea ice compared to the sea ice drafts of BGEP and NPI. Figure A5 displays the effect of the snow depth estimate of several snow depth products on the volume of sea ice, for both hemispheres.

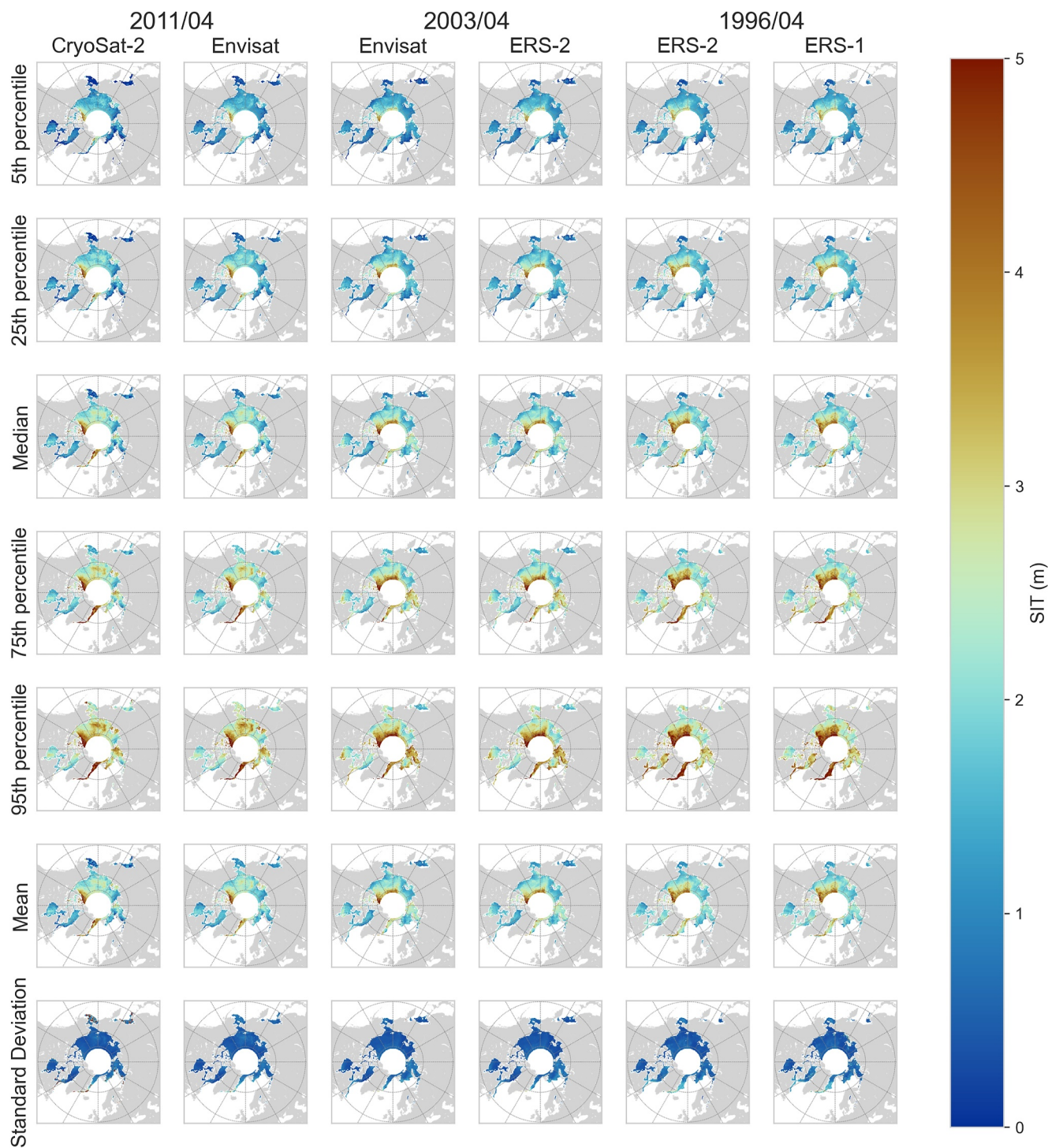


Figure A1. Statistics of Arctic sea ice thickness in March 2011, 2003, 1996 for each mission during each mission overlap period (CS-2, Envisat, ERS-2, ERS-1). Percentiles, mean and standard deviation.

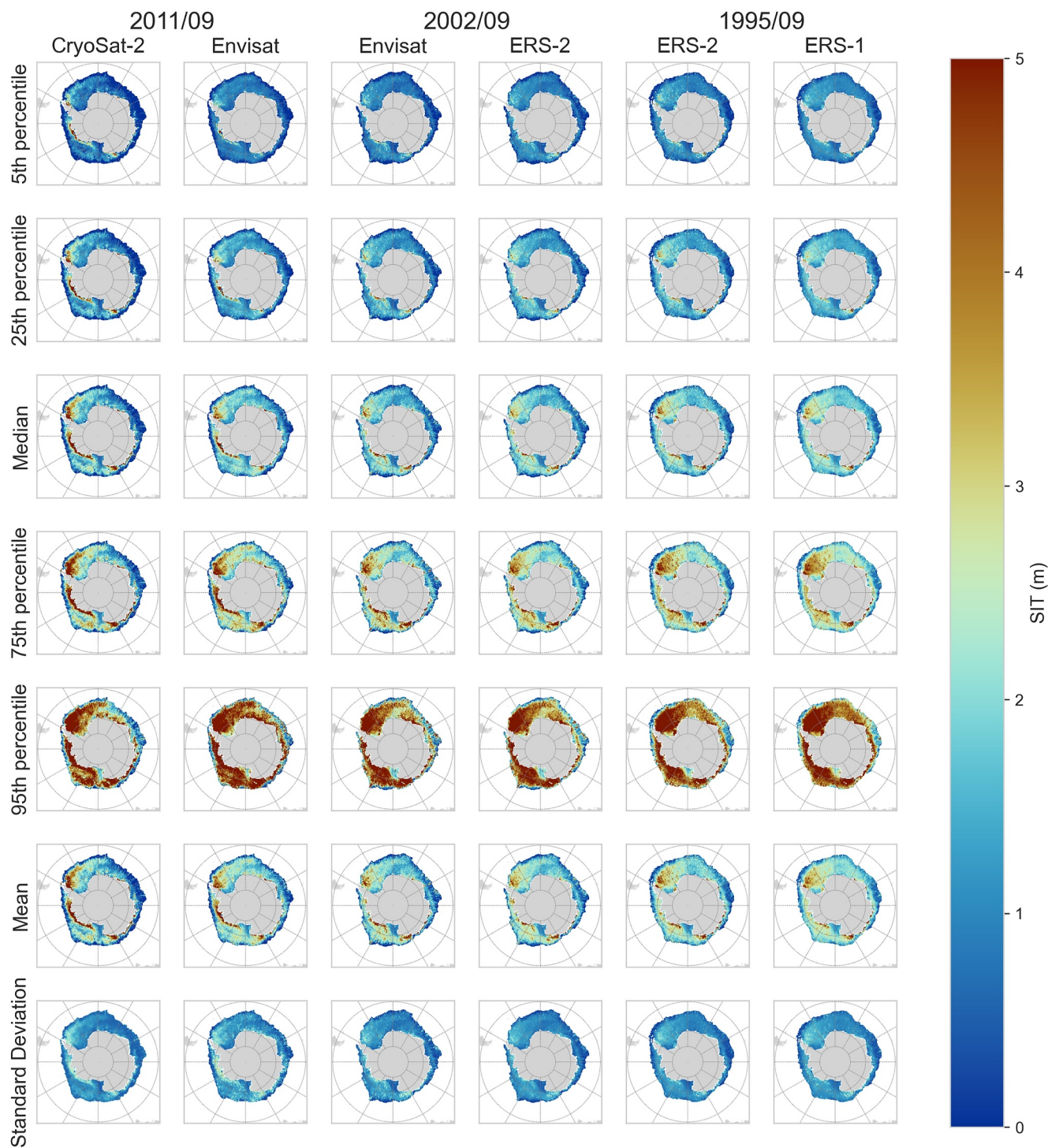


Figure A2. Statistics of Antarctic sea ice thickness for September 2011, 2002, 1995 for each mission during each mission overlap period (CS-2, Envisat, ERS-2, ERS-1). Percentiles, mean and standard deviation.

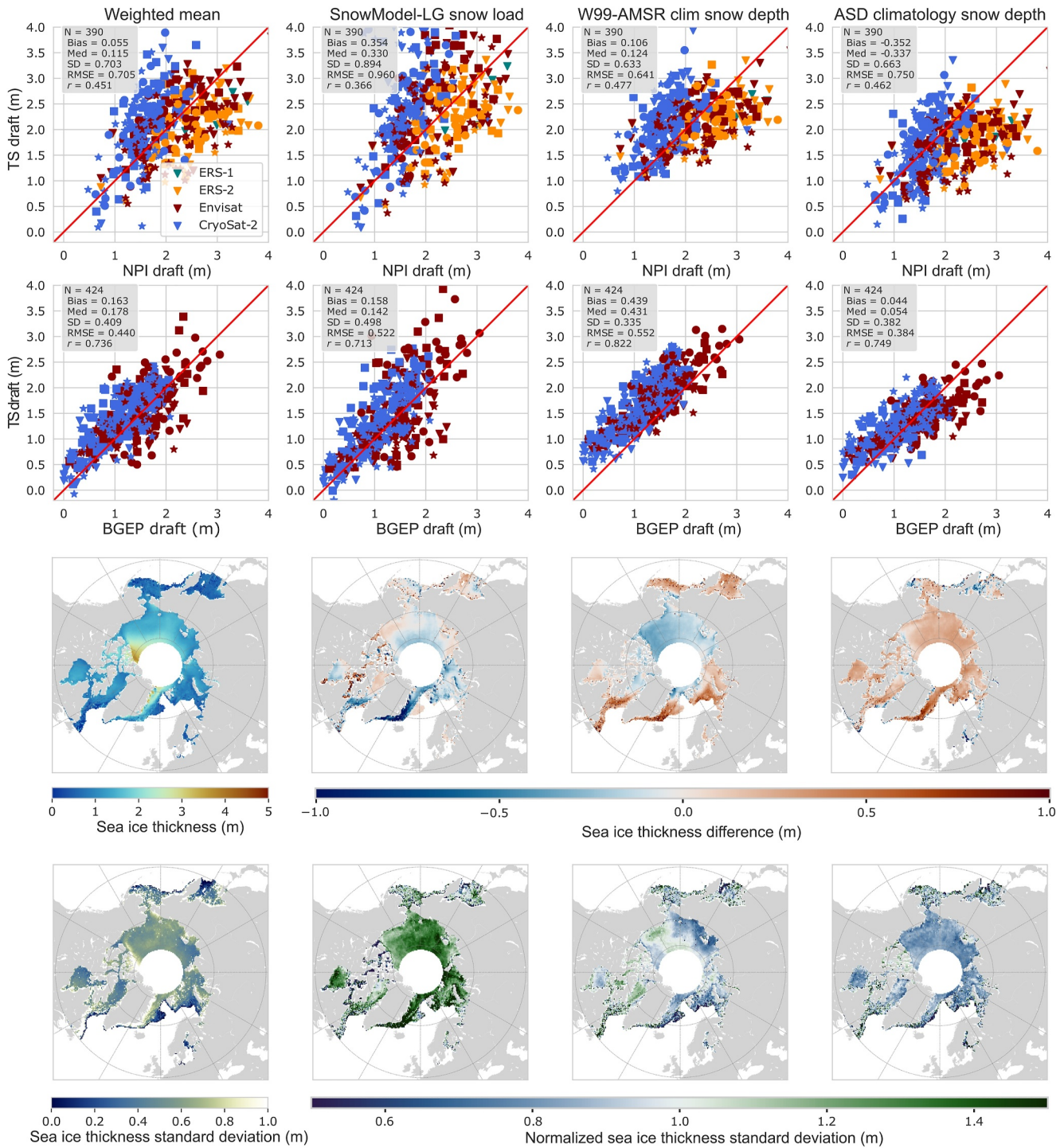


Figure A3. Sea ice thickness retrieval using the weighted mean of multiple snow depth products, SIT from SnowModel-LG ERA snow load, AMSRW99 and ASD climatology snow depth. The first two lines compare SIT for the NPI and BGEF mooring time series. The third line shows the mean sea ice thickness over 1994–2023 for the weighted mean and the bias on SIT computed with other snow depth products (Weighted mean—SIT from other snow depth products). The fourth line is the standard deviation of sea ice thickness for the weighted mean and the normalized standard deviation for the derived SIT with 3 other snow depths and the standard deviation of the SIT weighted mean (1994–2023).

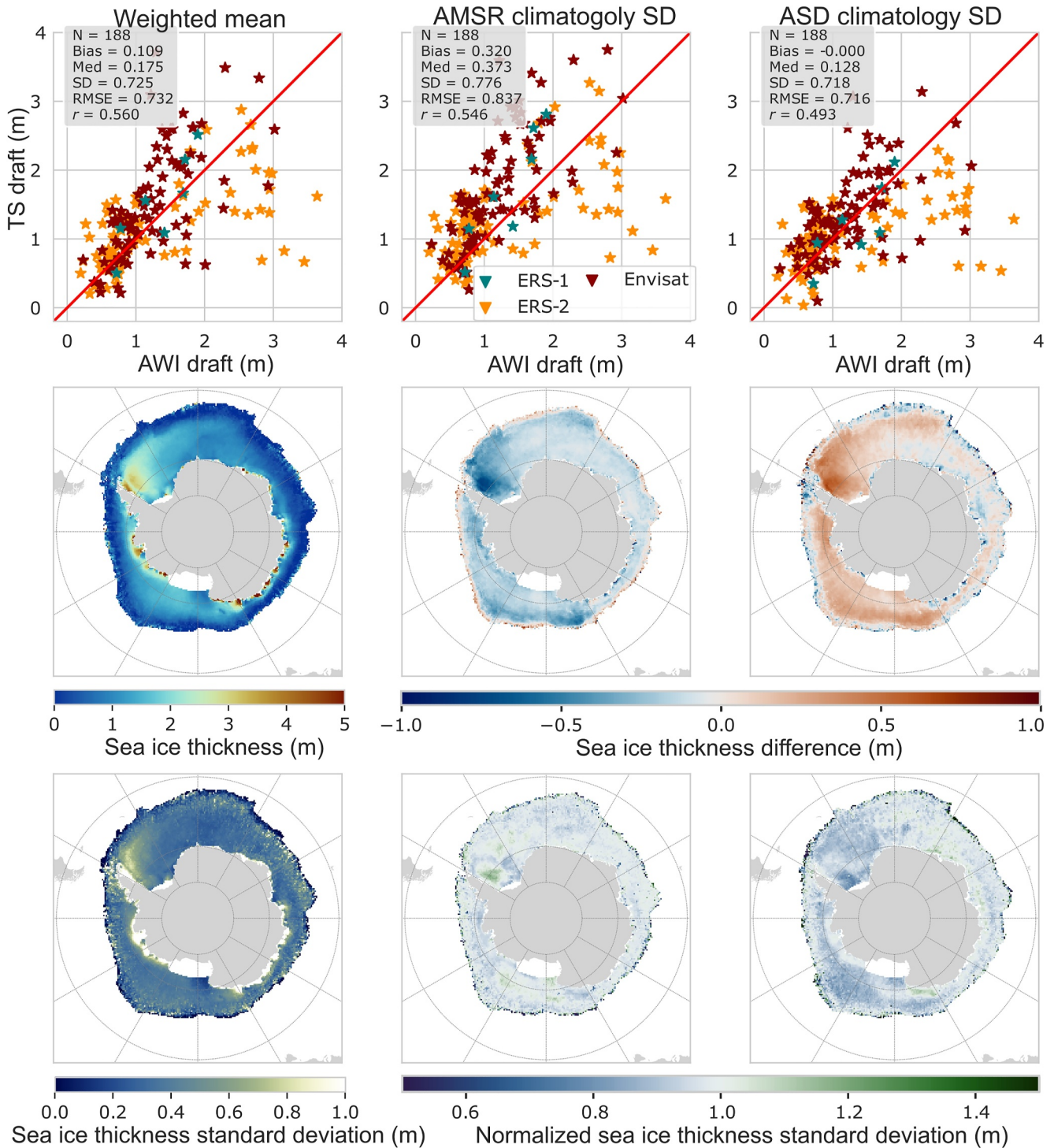


Figure A4. Sea ice thickness retrieval using the weighted mean of multiple snow depth products, SIT from AMSR, and ASD climatology snow depth. The first two lines compare SIT for the AWI mooring time series. The second line shows the mean sea ice thickness over 1994–2023 for the weighted mean and the bias on SIT computed with other snow depth products. The third line is the standard deviation of sea ice thickness for the weighted mean and the normalized standard deviation for the derived SIT with 2 other snow depth products and the standard deviation of the SIT weighted mean (1994–2023).

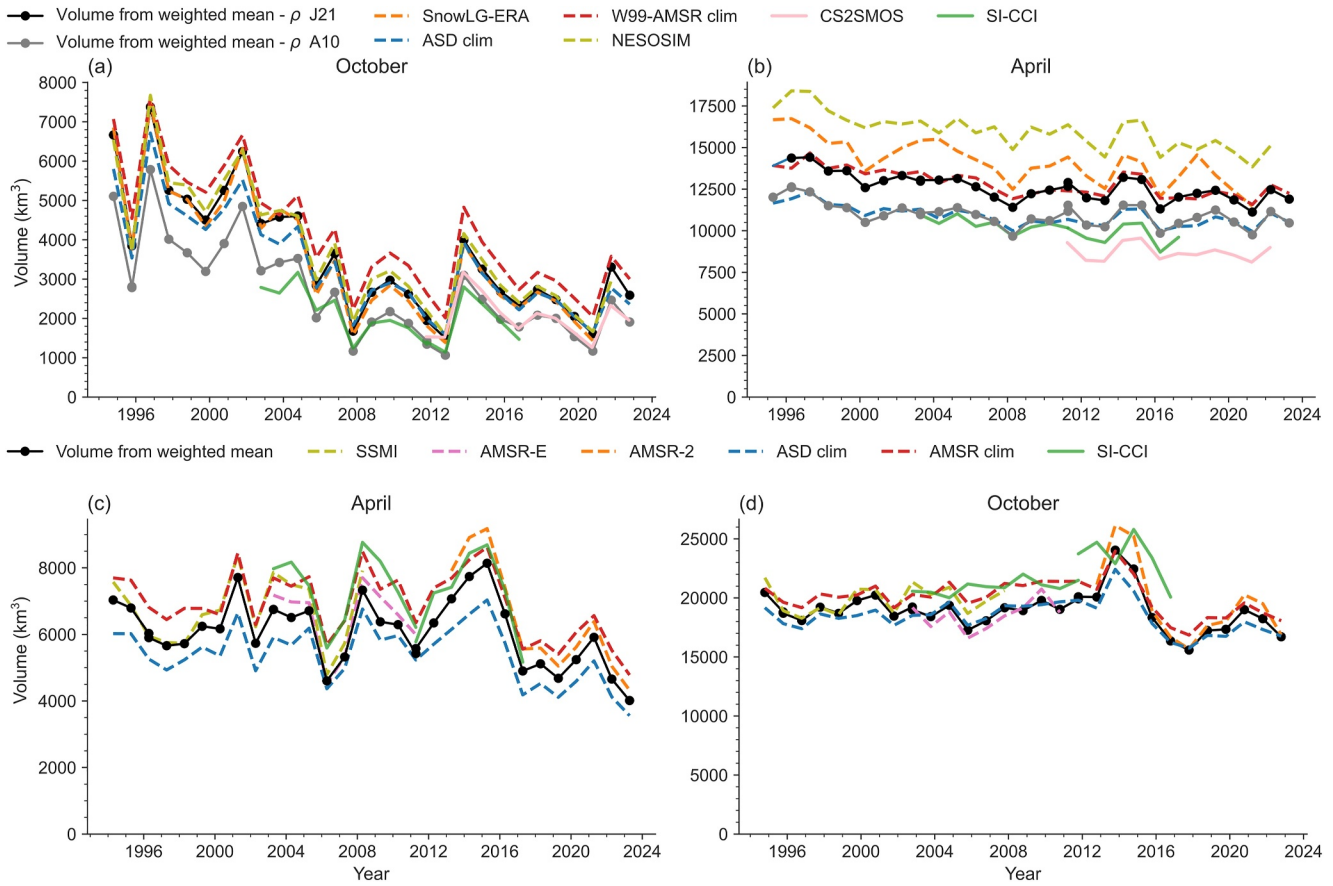


Figure A5. Arctic sea ice volume for October (a) and April (b) with the sea ice volume derived from the weighted mean SIT (black) for the 4 ESA missions with the sea ice density parameterization of Jutila et al. (2022) (J21) and Alexandrov et al. (2010) (A10) in gray. Sea ice volume time series computed with the ensemble of snow depth products used to generate the sea ice thickness ensemble (dashed lines). Satellite-derived sea ice volume from SI-CCI (green bold), CryoSat-2 with CS2SMOS (pink bold). Antarctic sea ice volume for April (c) and October (d) with sea ice volume derived from weight-averaged sea ice thickness (black) for the 4 ESA missions. Sea ice volume time series computed with each of the snow depth products used to generate the sea ice thickness ensemble (consideration of uncertainty) in dashed lines. Satellite derived sea ice volume from SI-CCI (green solid line).

Table A1
Arctic Sea Ice Volume Trends for Some of the Snow Depth Products Related to Figure A5

Sea ice volume label	October trend ($km^3/year$)	April trend ($km^3/year$)
SIV J21	-142.47	-78.14
SIV A10	-101.42	-52.23
SIV Snow-LG	-181.60	-139.60
SIV ASD clim	-122.82	-51.91
SIV W99-AMSR	-146.39	-76.45
SIV NESOSIM	-155.11	-104.32

Note. All trends are statistically significant ($1 - p\text{-value}$) > 0.95. Bold values correspond to volume derived from weighted mean sea ice thickness.

Appendix B: Monthly Sea Ice Thickness Trends and Monthly Volume Anomaly

Figures B1 and B2 represent sea ice thickness trends for each month (winter for NH and year round for SH). Figure B3 presents the volume anomaly for each regions and for both polar oceans.

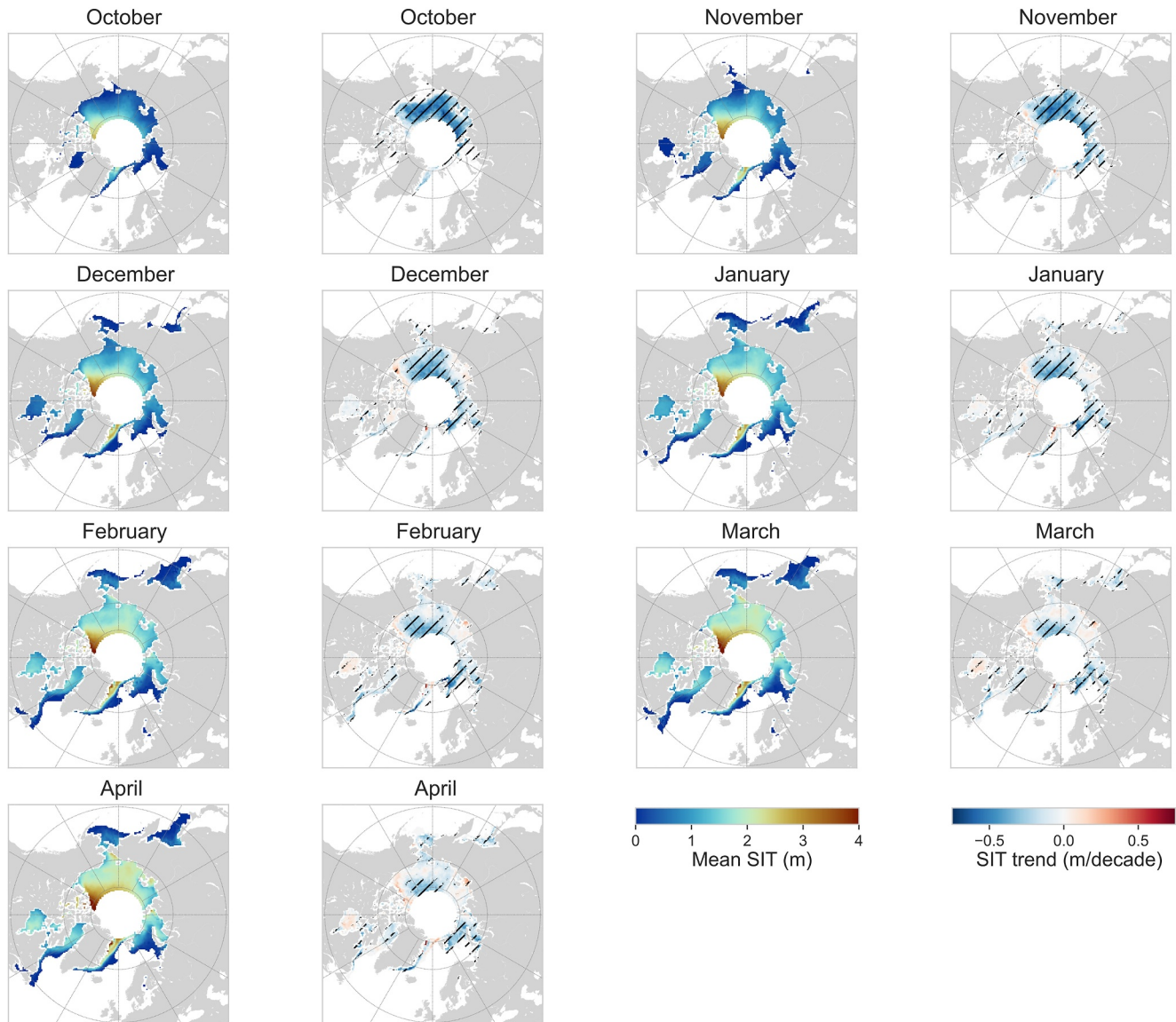


Figure B1. Mean Arctic sea ice thickness for all winter months (October–April) and associated trends. Winter months are shown from left to right and from top to bottom. Shaded areas on sea ice thickness trends represent regions where the trend is statistically significant with $(1 - p\text{-value}) > 0.95$.

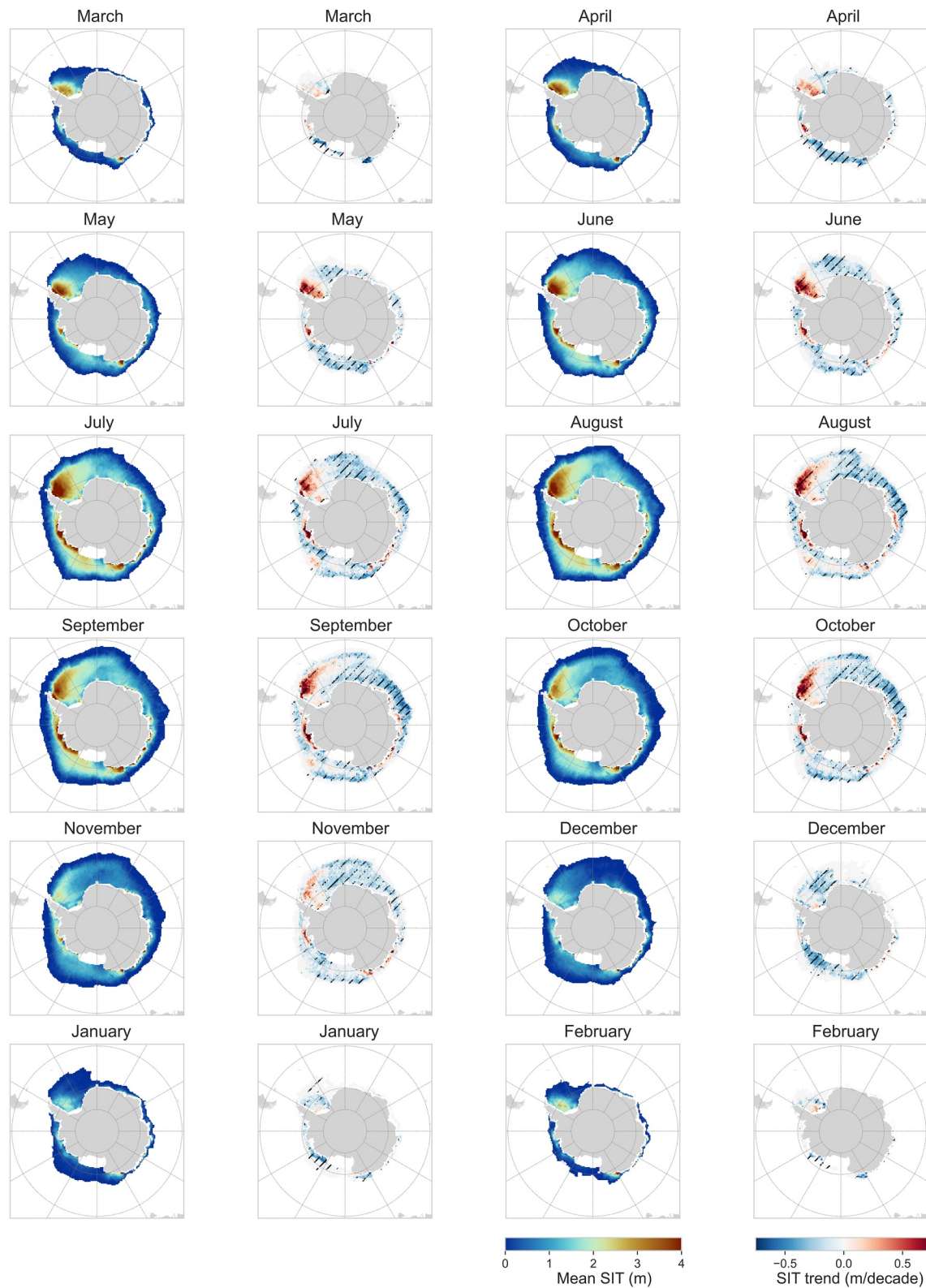


Figure B2. Mean Antarctic sea ice thickness for all months (March–February) and associated trends. Winter months from left to right and top to bottom. Shaded areas on sea ice thickness trends represent regions where the trend is statistically significant with $(1 - p\text{-value}) > 0.95$.

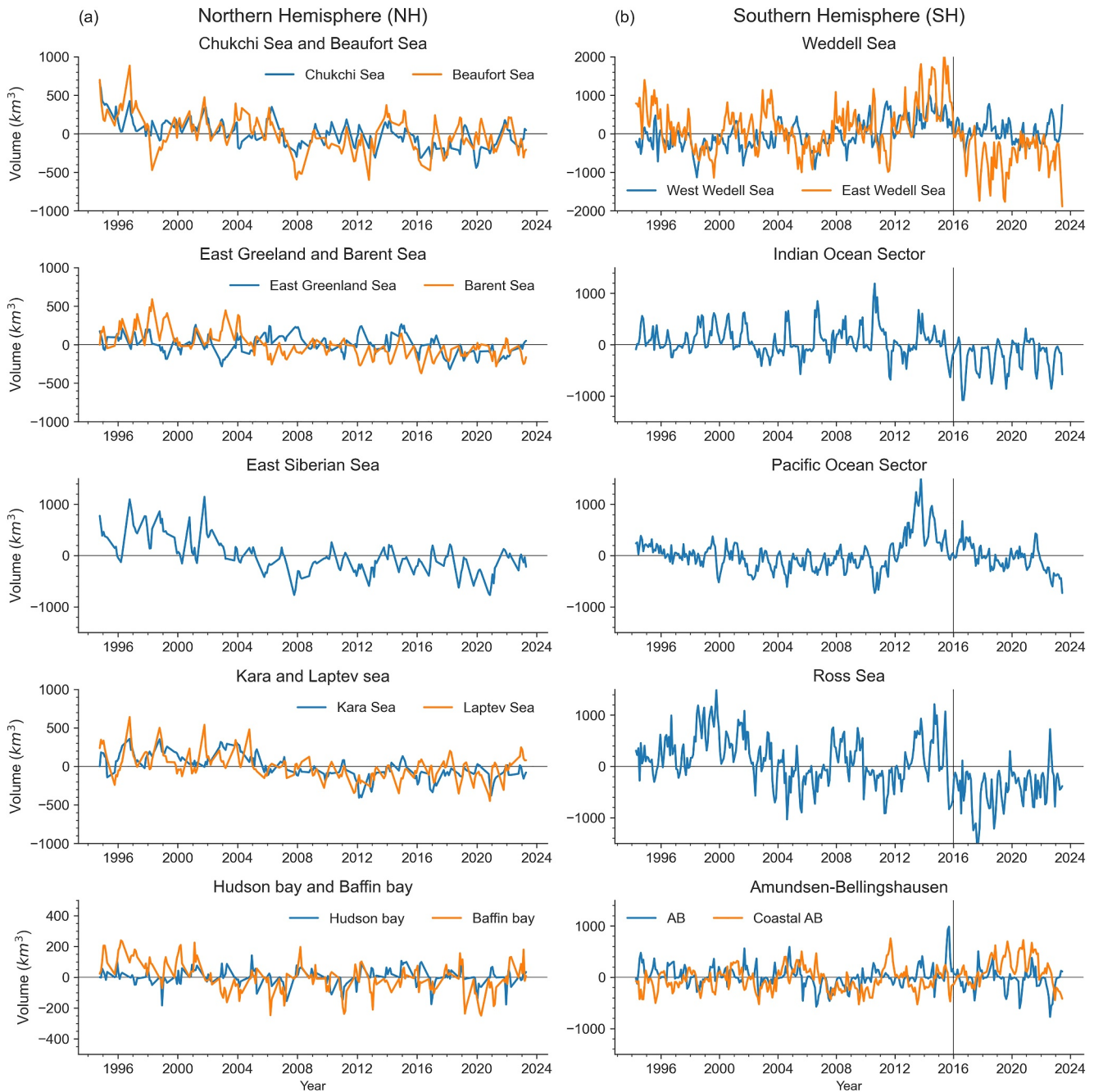


Figure B3. Sea ice volume anomaly for each region for both hemispheres with 1994–2023 as the reference period. Sea ice volume is limited where sea ice concentration is higher than 50%.

Data Availability Statement

The sea ice thickness time series for both hemispheres is available at <https://zenodo.org/records/12783561> (Bocquet et al., 2024). The code for generating the figures presented in this paper is available at the following GitHub repository: https://github.com/marionbocquet/TS_30years_NH_SH.git. The SI-CCI sea ice thickness v2.0 Envisat NH is available at <https://dx.doi.org/10.5285/f4c34f4f0f1d4d0da06d771f6972f180>, SH product is available at <https://dx.doi.org/10.5285/b1f1ac03077b4aa784c5a413a2210bf5>. For CryoSat-2 NH, the sea ice thickness is available at: <https://dx.doi.org/10.5285/ff79d140824f42dd92b204b4f1e9e7c2> and the SH data set at: <https://dx.doi.org/10.5285/48fc3d1e8ada405c8486ada522dae9e8>. CS2SMOS version v205 used in this study is

available at: <https://spaces.awi.de/pages/viewpage.action?pageId=291898639>. PIOMAS sea ice thickness version 2.1 is available at: <http://psc.apl.uw.edu/research/projects/arctic-sea-ice-volume-anomaly/data/model-grid>. GIOMAS sea ice thickness is available at: <http://psc.apl.washington.edu/zhang/Globalseaice/data.html>. CMIP6 models outputs (OMIP2 project) are available at: <https://esgf-node.llnl.gov/projects/cmip6/>. Operation Ice Bridge campaigns over Antarctic sea ice taken from: <https://nsidc.org/data/IDCSI4/versions/1>. AWI moorings sea ice draft available at: <https://doi.pangaea.de/10.1594/PANGAEA.785565>. BGEP sea ice draft available at: <https://www2.whoi.edu/site/beaufortgyre/data/mooring-data/>. NPI sea ice draft is available at: <https://data.npolar.no/dataset/b94cb848-3120-4f29-a827-298108e0d059>. SCICEX sea ice draft are taken from: <https://nsidc.org/data/g01360/versions/1>. Unified AMSRE/2 snow depth data set is taken from NSIDC version v1: <https://doi.org/10.5067/RA1MIJOYPK3P>.

Acknowledgments

This research was supported by the CNES (contract no. 3342) and CLS (contract no. CLS-ENV-BC-22-0221) thanks to a doctoral allowance granted to Marion Bocquet. This study was also supported by ESA in the framework of FDR4ALT project (contract no. 4000128220/19/I-B). The Scientific color map “roma” and “vik” (Cramer, 2021) are used in this study to prevent visual distortion of the data and exclusion of readers with color vision deficiencies (Cramer et al., 2020). The authors would like to thank Anne Liffermann for her support during the development of this work, as well as Florent Garnier for the enriching discussions and Camille Boulard for technical support. The authors also would like to acknowledge the editor as well as Stefan Hendricks and one anonymous referee for their valuable comments that helped to improve the paper.

References

- Aaboe, S., Down, E., Sørensen, A., Lavergne, T., & Eastwood, S. (2021). Sea-ice edge climate data record Oct1978-Aug2023. *Copernicus Climate Change Service (C3S) Climate Data Store (CDS)*. <https://doi.org/10.24381/CDS.29C46D83>
- Alexandrov, V., Sandven, S., Wahlin, J., & Johannessen, O. M. (2010). The relation between sea ice thickness and freeboard in the Arctic. *The Cryosphere*, 4(3), 373–380. <https://doi.org/10.5194/tc-4-373-2010>
- Behrendt, A., Dierking, W., Fahrbach, E., & Witte, H. (2013). Sea ice draft measured by upward looking sonars in the Weddell Sea (Antarctica). 38 datasets. <https://doi.org/10.1594/PANGAEA.785565>
- Bocquet, M., & Centre National d'Études Spatiales, & Laboratoire d'Études en Géophysique et Océanographie Spatiales. (2024). Arctic and Antarctic sea ice thickness climate data record from ERS-1, ERS-2, Envisat and CryoSat-2. *CNES-LEGOS*. <https://doi.org/10.5281/ZENODO.12783561>
- Bocquet, M., Fleury, S., Piras, F., Rinne, E., Sallila, H., Garnier, F., & Rémy, F. (2023). Arctic sea ice radar freeboard retrieval from the European Remote-Sensing Satellite (ERS-2) using altimetry: Toward sea ice thickness observation from 1995 to 2021. *The Cryosphere*, 17(7), 3013–3039. <https://doi.org/10.5194/tc-17-3013-2023>
- Boutin, G., Ólason, E., Rampal, P., Regan, H., Lique, C., Talandier, C., et al. (2023). Arctic sea ice mass balance in a new coupled ice–ocean model using a brittle rheology framework. *The Cryosphere*, 17(2), 617–638. <https://doi.org/10.5194/tc-17-617-2023>
- Cavalieri, D., Parkinson, C., Gloersen, P., & Zwally, H. J. (1996). Sea ice concentrations from Nimbus-7 SMMR and DMSP SSM/I-SSMIS passive microwave data, version 1. *NASA National Snow and Ice Data Center DAAC*. <https://doi.org/10.5067/8GQ8LZQVL0VL>
- Chelton, D. B., Walsh, E. J., & MacArthur, J. L. (1989). Pulse compression and sea level tracking in satellite altimetry. *Journal of Atmospheric and Oceanic Technology*, 6(3), 407–438. [https://doi.org/10.1175/1520-0426\(1989\)006<0407:PCASLT>2.0.CO;2](https://doi.org/10.1175/1520-0426(1989)006<0407:PCASLT>2.0.CO;2)
- Comiso, J., Cavalieri, D., & Markus, T. (2003). Sea ice concentration, ice temperature, and snow depth using AMSR-E data. *IEEE Transactions on Geoscience and Remote Sensing*, 41(2), 243–252. <https://doi.org/10.1109/TGRS.2002.808317>
- Comiso, J. C., Meier, W. N., & Gersten, R. (2017). Variability and trends in the Arctic Sea ice cover: Results from different techniques. *Journal of Geophysical Research: Oceans*, 122(8), 6883–6900. <https://doi.org/10.1002/2017JC012768>
- Cramer, F. (2021). Scientific colour maps. *Zenodo*. <https://doi.org/10.5281/ZENODO.1243862>
- Cramer, F., Shephard, G. E., & Heron, P. J. (2020). The misuse of colour in science communication. *Nature Communications*, 11(1), 5444. <https://doi.org/10.1038/s41467-020-19160-7>
- Dawson, A. (2016). eofs: A library for EOF analysis of meteorological, oceanographic, and climate data. *Journal of Open Research Software*, 4(1), 14. <https://doi.org/10.5334/jors.122>
- Eayrs, C., Li, X., Raphael, M. N., & Holland, D. M. (2021). Rapid decline in Antarctic sea ice in recent years hints at future change. *Nature Geoscience*, 14(7), 460–464. <https://doi.org/10.1038/s41561-021-00768-3>
- Fons, S., Kurtz, N., & Bagnardi, M. (2023). A decade-plus of Antarctic sea ice thickness and volume estimates from CryoSat-2 using a physical model and waveform fitting. *The Cryosphere*, 17(6), 2487–2508. <https://doi.org/10.5194/tc-17-2487-2023>
- Garnier, F., Bocquet, M., Fleury, S., Bouffard, J., Tsamados, M., Remy, F., et al. (2022). Latest altimetry-based sea ice freeboard and volume inter-annual variability in the Antarctic over 2003–2020. *Remote Sensing*, 14(19), 4741. <https://doi.org/10.3390/rs14194741>
- Garnier, F., Fleury, S., Garric, G., Bouffard, J., Tsamados, M., Laforge, A., et al. (2021). Advances in altimetric snow depth estimates using bi-frequency SARAL and CryoSat-2 Ka–Ku measurements. *The Cryosphere*, 15(12), 5483–5512. <https://doi.org/10.5194/tc-15-5483-2021>
- Ghantous, M., Ayoub, N., De Mey-Frémaux, P., Vervatis, V., & Marsaleix, P. (2020). Ensemble downscaling of a regional ocean model. *Ocean Modelling*, 145, 101511. <https://doi.org/10.1016/j.ocemod.2019.101511>
- Giles, K. A., Laxon, S. W., & Worby, A. P. (2008). Antarctic sea ice elevation from satellite radar altimetry. *Geophysical Research Letters*, 35(3), L03503. <https://doi.org/10.1029/2007GL031572>
- Guerreiro, K., Fleury, S., Zakharova, E., Kouraev, A., Rémy, F., & Maisongrande, P. (2017). Comparison of CryoSat-2 and ENVISAT radar freeboard over Arctic sea ice: Toward an improved Envisat freeboard retrieval. *The Cryosphere*, 11(5), 2059–2073. <https://doi.org/10.5194/tc-11-2059-2017>
- Haumann, F. A., Gruber, N., Münnich, M., Frenger, I., & Kern, S. (2016). Sea-ice transport driving Southern Ocean salinity and its recent trends. *Nature*, 537(7618), 89–92. <https://doi.org/10.1038/nature19101>
- Haumann, F. A., Notz, D., & Schmidt, H. (2014). Anthropogenic influence on recent circulation-driven Antarctic sea ice changes. *Geophysical Research Letters*, 41(23), 8429–8437. <https://doi.org/10.1002/2014GL061659>
- Helm, V., Humbert, A., & Miller, H. (2014). Elevation and elevation change of Greenland and Antarctica derived from CryoSat-2. *The Cryosphere*, 8(4), 1539–1559. <https://doi.org/10.5194/tc-8-1539-2014>
- Hendricks, S., Paul, S., & Rinne, E. (2018a). ESA Sea Ice Climate Change Initiative (Sea_ice_cci): Northern hemisphere sea ice thickness from the CryoSat-2 satellite on a monthly grid (L3C), v2.0. [Object Object]. <https://doi.org/10.5285/FF79D140824F42DD92B204B4F1E9E7C2>
- Hendricks, S., Paul, S., & Rinne, E. (2018b). ESA Sea Ice Climate Change Initiative (Sea_ice_cci): Northern hemisphere sea ice thickness from the Envisat satellite on a monthly grid (L3C), v2.0. [Object Object]. <https://doi.org/10.5285/F4C34F40F1D4D0DA06D771F6972F180>
- Hendricks, S., Paul, S., & Rinne, E. (2018c). ESA Sea Ice Climate Change Initiative (Sea_ice_cci): Southern hemisphere sea ice thickness from the CryoSat-2 satellite on a monthly grid (L3C), v2.0. [Object Object]. <https://doi.org/10.5285/48FC3D1E8ADA405C8486ADA522DAE9E8>

- Hendricks, S., Paul, S., & Rinne, E. (2018d). ESA Sea Ice Climate Change Initiative (Sea_ice_cci): Southern hemisphere sea ice thickness from the Envisat satellite on a monthly grid (L3C), v2.0. [Object Object]. <https://doi.org/10.5285/B1F1AC03077B4AA784C5A413A2210BF5>
- Holland, P. R., Bruneau, N., Enright, C., Losch, M., Kurtz, N. T., & Kwok, R. (2014). Modeled trends in Antarctic sea ice thickness. *Journal of Climate*, 27(10), 3784–3801. <https://doi.org/10.1175/JCLI-D-13-00301.1>
- Holland, P. R., & Kimura, N. (2016). Observed concentration budgets of Arctic and Antarctic sea ice. *Journal of Climate*, 29(14), 5241–5249. <https://doi.org/10.1175/JCLI-D-16-0121.1>
- Jutila, A., Hendricks, S., Ricker, R., von Albedyll, L., Krumpfen, T., & Haas, C. (2022). Retrieval and parameterisation of sea-ice bulk density from airborne multi-sensor measurements. *The Cryosphere*, 16(1), 259–275. <https://doi.org/10.5194/tc-16-259-2022>
- Kacimi, S., & Kwok, R. (2020). The Antarctic sea ice cover from ICESat-2 and CryoSat-2: Freeboard, snow depth, and ice thickness. *The Cryosphere*, 14(12), 4453–4474. <https://doi.org/10.5194/tc-14-4453-2020>
- Kendall, M. G. (1948). Rank correlation methods.
- Kern, S. (2020). ESA-CCI_phase2_standardized_manual_visual_ship-Based_seaiceobservations_v02. *World Data Center for Climate (WDCC) at DKRZ*. <https://doi.org/10.26050/WDCC/ESACIPSMVBSIOV2>
- Kern, S., Ozsoy-Çiçek, B., & Worby, A. P. (2016). Antarctic sea-ice thickness retrieval from ICESat: Inter-comparison of different approaches. *Remote Sensing*, 8(7), 538. <https://doi.org/10.3390/rs8070538>
- Kim, Y.-H., Min, S.-K., Gillett, N. P., Notz, D., & Malinina, E. (2023). Observationally-constrained projections of an ice-free Arctic even under a low emission scenario. *Nature Communications*, 14(1), 3139. <https://doi.org/10.1038/s41467-023-38511-8>
- Kurtz, N., Studinger, M., Harbeck, J., DePaul Onana, V., & Yi, D. (2015). IceBridge L4 sea ice freeboard, snow depth, and thickness, version 1. [Object Object]. <https://doi.org/10.5067/G519SHCKWQV6>
- Kurtz, N. T., & Farrell, S. L. (2011). Large-scale surveys of snow depth on Arctic sea ice from Operation IceBridge. *Geophysical Research Letters*, 38(20), L20505. <https://doi.org/10.1029/2011GL049216>
- Kurtz, N. T., & Markus, T. (2012). Satellite observations of Antarctic sea ice thickness and volume: Antarctic sea ice thickness. *Journal of Geophysical Research*, 117(C8), C08025. <https://doi.org/10.1029/2012JC008141>
- Kwok, R. (2018). Arctic sea ice thickness, volume, and multiyear ice coverage: Losses and coupled variability (1958–2018). *Environmental Research Letters*, 13(10), 105005. <https://doi.org/10.1088/1748-9326/aae3ec>
- Kwok, R., Cunningham, G. F., Wensnahan, M., Rigor, I., Zwally, H. J., & Yi, D. (2009). Thinning and volume loss of the Arctic Ocean sea ice cover: 2003–2008. *Journal of Geophysical Research*, 114(C7), C07005. <https://doi.org/10.1029/2009JC005312>
- Kwok, R., Kacimi, S., Webster, M., Kurtz, N., & Petty, A. (2020). Arctic snow depth and sea ice thickness from ICESat-2 and CryoSat-2 freeboards: A first examination. *Journal of Geophysical Research: Oceans*, 125(3), e2019JC016008. <https://doi.org/10.1029/2019JC016008>
- Landy, J. C., Dawson, G. J., Tsamados, M., Bushuk, M., Stroeve, J. C., Howell, S. E. L., et al. (2022). A year-round satellite sea-ice thickness record from CryoSat-2. *Nature*, 609(7927), 517–522. <https://doi.org/10.1038/s41586-022-05058-5>
- Landy, J. C., Tsamados, M., & Scharien, R. K. (2019). A facet-based numerical model for simulating SAR altimeter echoes from heterogeneous sea ice surfaces. *IEEE Transactions on Geoscience and Remote Sensing*, 57(7), 4164–4180. <https://doi.org/10.1109/TGRS.2018.2889763>
- Laxon, S. (1994). Sea ice altimeter processing scheme at the EODC. *International Journal of Remote Sensing*, 15(4), 915–924. <https://doi.org/10.1080/01431169408954124>
- Laxon, S., Peacock, N., & Smith, D. (2003). High interannual variability of sea ice thickness in the Arctic region. *Nature*, 425(6961), 947–950. <https://doi.org/10.1038/nature02050>
- Laxon, S. W., Giles, K. A., Ridout, A. L., Wingham, D. J., Willatt, R., Cullen, R., et al. (2013). CryoSat-2 estimates of Arctic sea ice thickness and volume. *Geophysical Research Letters*, 40(4), 732–737. <https://doi.org/10.1002/grl.50193>
- Liston, G., Stroeve, J., & Itkin, P. (2020). Lagrangian snow distributions for sea-ice applications. *NASA National Snow and Ice Data Center DAAC*. <https://doi.org/10.5067/27A0P5M6LZBI>
- Maksym, T., & Markus, T. (2008). Antarctic sea ice thickness and snow-to-ice conversion from atmospheric reanalysis and passive microwave snow depth. *Journal of Geophysical Research*, 113(C2), C02S12. <https://doi.org/10.1029/2006JC004085>
- Maksym, T., Stammerjohn, S., Ackley, S., & Massom, R. (2012). Antarctic sea ice—A polar opposite? *Oceanography*, 25(3), 140–151. <https://doi.org/10.5670/oceanog.2012.88>
- Mallett, R. D. C., Lawrence, I. R., Stroeve, J. C., Landy, J. C., & Tsamados, M. (2020). Brief communication: Conventional assumptions involving the speed of radar waves in snow introduce systematic underestimates to sea ice thickness and seasonal growth rate estimates. *The Cryosphere*, 14(1), 251–260. <https://doi.org/10.5194/tc-14-251-2020>
- Mann, H. (1945). Nonparametric tests against trend. *Econometrica: Journal of the Econometric Society*, 13(3), 245–259. <https://doi.org/10.2307/1907187>
- Markus, T., & Cavalieri, D. J. (2013). Snow depth distribution over sea ice in the Southern Ocean from satellite passive microwave data. In M. O. Jeffries (Ed.), *Antarctic research series* (pp. 19–39). American Geophysical Union. <https://doi.org/10.1029/AR074p0019>
- Massonnet, F., Mathiot, P., Fichet, T., Goosse, H., König Beatty, C., Vancoppenolle, M., & Lavergne, T. (2013). A model reconstruction of the Antarctic sea ice thickness and volume changes over 1980–2008 using data assimilation. *Ocean Modelling*, 64, 67–75. <https://doi.org/10.1016/j.ocemod.2013.01.003>
- Meier, W. (2017). AMSR-E/AMSR2 unified L3 daily 12.5 km polar gridded brightness temperatures, sea ice concentration, & snow depth, version 1. [Object Object]. <https://doi.org/10.5067/RA1MJJOYPK3P>
- Meier, W., Fetterer, F., Windnagel, A., & Stewart, S. (2021). NOAA/NSIDC climate data record of passive microwave sea ice concentration, version 4. *NSIDC*. <https://doi.org/10.7265/EFMZ-2T65>
- Meier, W. N., Hovelsrud, G. K., van Oort, B. E., Key, J. R., Kovacs, K. M., Michel, C., et al. (2014). Arctic sea ice in transformation: A review of recent observed changes and impacts on biology and human activity: Arctic sea ice: Review of recent changes. *Reviews of Geophysics*, 52(3), 185–217. <https://doi.org/10.1002/2013RG000431>
- Meredith, M., Sommerkom, M., Cassotta, S., Derksen, C., Ekaykin, A., Hollowed, A., et al. (2019). Polar regions. In *IPCC special report on the ocean and cryosphere in a changing climate* (1st ed.). Cambridge University Press. <https://doi.org/10.1017/9781009157964>
- National Snow and Ice Data Center (Comp.). (1998). *Submarine upward looking sonar ice draft profile data and statistics, version 1*. National Snow and Ice Data Center. <https://doi.org/10.7265/N54Q7RWK>
- Notz, D., & SIMIP Community (2020). Arctic sea ice in CMIP6. *Geophysical Research Letters*, 47(10), e2019GL086749. <https://doi.org/10.1029/2019GL086749>
- OSI SAF. (2022a). GBL SICO CDR R3Global sea ice concentration climate data record v3.0—Multimission. *OSI SAF*. https://doi.org/10.15770/EUM_SAF_OSI_0013
- OSI SAF. (2022b). OSI-430-aGlobal sea ice concentration interim climate data record release 3—DMSP. *OSI SAF*. https://doi.org/10.15770/EUM_SAF_OSI_0014

- Paul, S., Hendricks, S., Ricker, R., Kern, S., & Rinne, E. (2018). Empirical parametrization of Envisat freeboard retrieval of Arctic and Antarctic sea ice based on CryoSat-2: Progress in the ESA climate change initiative. *The Cryosphere*, *12*(7), 2437–2460. <https://doi.org/10.5194/tc-12-2437-2018>
- Paul, S., Sallila, H., Hendricks, S., & Rinne, E. (2021). ESA CCI+ climate change initiative phase 1, D2.1 sea ice thickness Algorithm theoretical basis document (ATBD), v.3.1 (Technical Report). Retrieved from <https://climate.esa.int/en/projects/sea-ice/Sea-Ice-Key-Documents/>
- Peacock, N. R., & Laxon, S. W. (2004). Sea surface height determination in the Arctic Ocean from ERS altimetry. *Journal of Geophysical Research*, *109*(C7), C07001. <https://doi.org/10.1029/2001JC001026>
- Petty, A. A., Webster, M., Boisvert, L., & Markus, T. (2018). The NASA Eulerian snow on sea ice model (NESOSIM) v1.0: Initial model development and analysis. *Geoscientific Model Development*, *11*(11), 4577–4602. <https://doi.org/10.5194/gmd-11-4577-2018>
- Purich, A., & Doddridge, E. W. (2023). Record low Antarctic sea ice coverage indicates a new sea ice state. *Communications Earth & Environment*, *4*(1), 1–9. <https://doi.org/10.1038/s43247-023-00961-9>
- Raney, R. (1998). The delay/Doppler radar altimeter. *IEEE Transactions on Geoscience and Remote Sensing*, *36*(5), 1578–1588. <https://doi.org/10.1109/36.718861>
- Ricker, R., Girard-Arduin, F., Krumpen, T., & Lique, C. (2018). Satellite-derived sea ice export and its impact on Arctic ice mass balance. *The Cryosphere*, *12*(9), 3017–3032. <https://doi.org/10.5194/tc-12-3017-2018>
- Ricker, R., Hendricks, S., Girard-Arduin, F., Kaleschke, L., Lique, C., Tian-Kunze, X., et al. (2017). Satellite-observed drop of Arctic sea ice growth in winter 2015–2016. *Geophysical Research Letters*, *44*(7), 3236–3245. <https://doi.org/10.1002/2016GL072244>
- Rothrock, D. A., Yu, Y., & Maykut, G. A. (1999). Thinning of the Arctic sea-ice cover. *Geophysical Research Letters*, *26*(23), 3469–3472. <https://doi.org/10.1029/1999GL010863>
- Schwegmann, S., Rinne, E., Ricker, R., Hendricks, S., & Helm, V. (2016). About the consistency between Envisat and CryoSat-2 radar freeboard retrieval over Antarctic sea ice. *The Cryosphere*, *10*(4), 1415–1425. <https://doi.org/10.5194/tc-10-1415-2016>
- Sen, P. K. (1968). Estimates of the regression coefficient based on Kendall's tau. *Journal of the American Statistical Association*, *63*(324), 1379–1389. <https://doi.org/10.2307/2285891>
- Stammerjohn, S., Massom, R., Rind, D., & Martinson, D. (2012). Regions of rapid sea ice change: An inter-hemispheric seasonal comparison. *Geophysical Research Letters*, *39*(6), L06501. <https://doi.org/10.1029/2012GL050874>
- Stroeve, J., Liston, G. E., Buzzard, S., Zhou, L., Mallett, R., Barrett, A., et al. (2020). A Lagrangian snow evolution system for sea ice applications (SnowModel-LG): Part II—Analyses. *Journal of Geophysical Research: Oceans*, *125*(10), e2019JC015900. <https://doi.org/10.1029/2019JC015900>
- Stroeve, J., & Notz, D. (2018). Changing state of Arctic sea ice across all seasons. *Environmental Research Letters*, *13*(10), 103001. <https://doi.org/10.1088/1748-9326/aade56>
- Sumata, H., de Steur, L., Divine, D. V., Granskog, M. A., & Gerland, S. (2023). Regime shift in Arctic Ocean sea ice thickness. *Nature*, *615*(7952), 443–449. <https://doi.org/10.1038/s41586-022-05686-x>
- Theil, H. (1950). A rank-invariant method of linear and polynomial regression analysis. *Indagationes mathematicae*, *12*(85), 173.
- Tilling, R., Ridout, A., & Shepherd, A. (2019). Assessing the impact of lead and floe sampling on Arctic sea ice thickness estimates from Envisat and CryoSat-2. *Journal of Geophysical Research: Oceans*, *124*(11), 7473–7485. <https://doi.org/10.1029/2019JC015232>
- Tilling, R. L., Ridout, A., & Shepherd, A. (2018). Estimating Arctic sea ice thickness and volume using CryoSat-2 radar altimeter data. *Advances in Space Research*, *62*(6), 1203–1225. <https://doi.org/10.1016/j.asr.2017.10.051>
- Tilling, R., Ridout, A., Shepherd, A., & Wingham, D. J. (2015). Increased Arctic sea ice volume after anomalously low melting in 2013. *Nature Geoscience*, *8*(8), 643–646. (MAG ID: 971406924). <https://doi.org/10.1038/ngeo2489>
- Ulaby, F. T., Moore, R. K., & Fung, A. K. (1986). Microwave remote sensing: Active and passive, Volume 3-From theory to applications. <https://doi.org/10.1017/S0016756800015831>
- Vervatis, V., Testut, C., De Mey, P., Ayoub, N., Chanut, J., & Quattrocchi, G. (2016). Data assimilative twin-experiment in a high-resolution Bay of Biscay configuration: 4DEnOI based on stochastic modeling of the wind forcing. *Ocean Modelling*, *100*, 1–19. <https://doi.org/10.1016/j.ocemod.2016.01.003>
- Warren, S. G., Rigor, I. G., Untersteiner, N., Radionov, V. F., Bryazgin, N. N., Aleksandrov, Y. I., & Colony, R. (1999). Snow depth on Arctic sea ice. *Journal of Climate*, *12*(6), 1814–1829. [https://doi.org/10.1175/1520-0442\(1999\)012<1814:SDOASI>2.0.CO;2](https://doi.org/10.1175/1520-0442(1999)012<1814:SDOASI>2.0.CO;2)
- Worby, A. P., Geiger, C. A., Paget, M. J., Van Woert, M. L., Ackley, S. F., & DeLiberty, T. L. (2008). Thickness distribution of Antarctic sea ice. *Journal of Geophysical Research*, *113*(C5), C05S92. <https://doi.org/10.1029/2007JC004254>
- Zhang, J., & Rothrock, D. A. (2003). Modeling global sea ice with a thickness and enthalpy distribution model in generalized curvilinear coordinates. *Monthly Weather Review*, *131*(5), 845–861. [https://doi.org/10.1175/1520-0493\(2003\)131<0845:MGSIIWA>2.0.CO;2](https://doi.org/10.1175/1520-0493(2003)131<0845:MGSIIWA>2.0.CO;2)
- Zhou, L., Stroeve, J., Xu, S., Petty, A., Tilling, R., Winstrup, M., et al. (2021). Inter-comparison of snow depth over Arctic sea ice from reanalysis reconstructions and satellite retrieval. *The Cryosphere*, *15*(1), 345–367. <https://doi.org/10.5194/tc-15-345-2021>